cmgh
CELLULAR AND MOLECULAR GASTROENTEROLOGY AND HEPATOLOGY

ORIGINAL RESEARCH

Human Fetal-Derived Enterospheres Provide Insights on Intestinal Development and a Novel Model to Study Necrotizing Enterocolitis (NEC)

Stefania Senger,[1,2] Laura Ingano,[1] Rachel Freire,[1] Antony Anselmo,[3] Weishu Zhu,[1] Ruslan Sadreyev,[3] William Allan Walker,[1,2,§] and Alessio Fasano[1,2,§]

[1]*Department of Pediatrics, Mucosal Immunology and Biology Research Center,* [3]*Department of Molecular Biology, Cancer Center and Center for Regenerative Medicine, Massachusetts General Hospital, Boston, Massachusetts;* [2]*Harvard Medical School, Boston, Massachusetts*

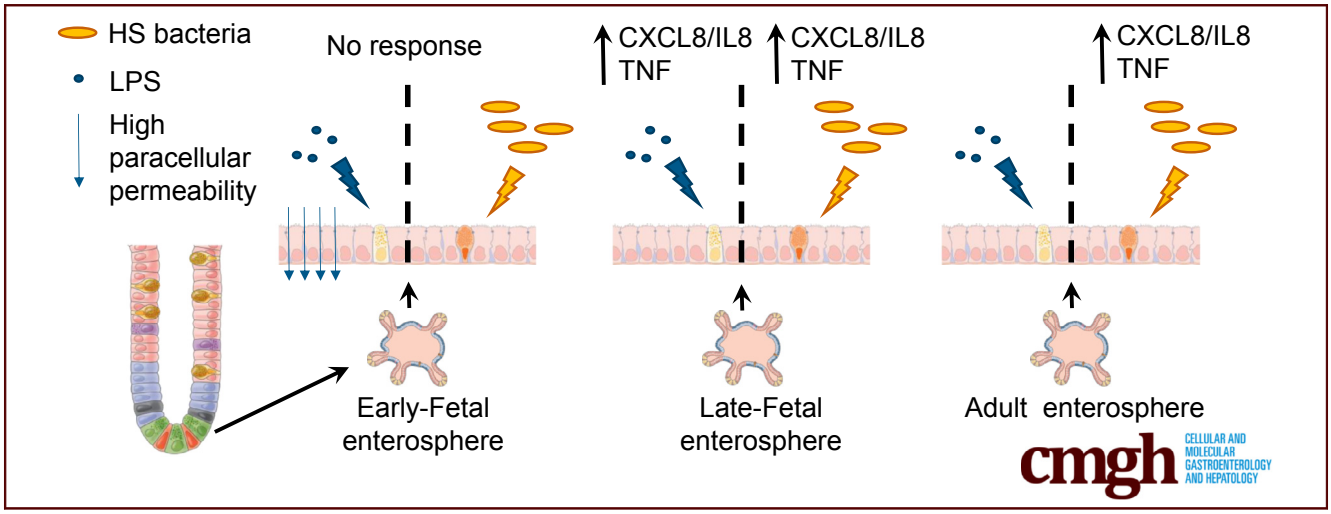

SUMMARY

We established enterospheres from human fetuses ranging from 11 to 22.5 weeks' gestational age. Developmentally regulated differences in maturation, barrier, and innate immunity were found across the samples. Fetal enterospheres can be used as a model for necrotizing enterocolitis pathogenesis.

BACKGROUND & AIMS: Untreated necrotizing enterocolitis (NEC) can lead to massive inflammation resulting in intestinal necrosis with a high mortality rate in preterm infants. Limited access to human samples and relevant experimental models have hampered progress in NEC pathogenesis. Earlier evidence has suggested that bacterial colonization of an immature and developing intestine can lead to an abnormally high inflammatory response to bacterial bioproducts. The aim of our study was to use human fetal organoids to gain insights into NEC pathogenesis.

METHODS: RNA sequencing analysis was performed to compare patterns of gene expression in human fetal-derived enterospheres (FEnS) and adult-derived enterospheres (AEnS). Differentially expressed genes were analyzed using computational techniques for dimensional reduction, clustering, and gene set enrichment. Unsupervised cluster analysis, Gene Ontology, and gene pathway analysis were used to predict differences between gene expression of samples. Cell monolayers derived from FEnS and AEnS were evaluated for epithelium function and responsiveness to lipopolysaccharide and commensal bacteria.

RESULTS: Based on gene expression patterns, FEnS clustered according to their developmental age in 2 distinct groups: early and late FEnS, with the latter more closely resembling AEnS. Genes involved in maturation, gut barrier function, and innate immunity were responsible for these differences. FEnS-derived monolayers exposed to either lipopolysaccharide or commensal *Escherichia coli* showed that late FEnS activated gene expression of key inflammatory cytokines, whereas early FEnS monolayers did not, owing to decreased expression of nuclear factor-κB–associated machinery.

CONCLUSIONS: Our results provide insights into processes underlying human intestinal development and support the use of FEnS as a relevant human preclinical model for NEC. Accession number of repository for expression data: GSE101531. *(Cell Mol Gastroenterol Hepatol 2018;5:549–568; https://doi.org/10.1016/j.jcmgh.2018.01.014)*

Keywords: Necrotizing Enterocolitis; Fetal Organoids; Enteroids.

See editorial on page 651.

Necrotizing enterocolitis (NEC) is the most frequent cause of death in premature infants in North America,[1,2] affecting more than 10% of premature babies weighing less than 1500 g, with an average cost of US $500,000 per patient.[3] NEC is characterized by severe inflammation of the gastrointestinal tract, leading to extensive tissue necrosis.[4] Despite several decades of basic and clinical research into NEC, the mortality rate and disease management has not changed appreciably over time. Currently, there is no Food and Drug Administration–approved treatment protocol to manage the disease,[5] with the exception of providing the infant with mother's expressed breast milk.[6] Nonetheless, in the past decade, intensive research efforts using techniques such as animal models, fetal intestinal xenograft transplants, fetal intestinal organ cultures, and a fetal primary intestinal cell line have shown that an abnormal response to gut-colonizing bacteria seems to contribute to NEC susceptibility.[7–9] In particular, the high incidence of NEC among very premature infants implicates intestinal immaturity as an additional risk factor.[10] Studies have shown that the immature human enterocyte reacts to colonizing intestinal bacteria with an enhanced inflammatory response.[11–13] Toll-like receptors (TLRs) have been implicated as key molecules in promoting inflammation.[14] In particular, TLR4 has been found to be up-regulated on the fetal enterocyte surface.[15] Similarly, other signaling factors connecting TLR4 to nuclear factor-κB (NF-κB) and activator protein transcription factor–mediated inflammation were found to be up-regulated as well, whereas genes that inhibited these signaling pathways were down-regulated.[11,16] Together this evidence suggests that an exaggerated innate immune response to colonizing commensal bacteria mediated by TLR activation is mounted by immature intestinal epithelial cells, which could contribute to the pathogenesis of NEC.

A major roadblock in determining the pathogenesis of NEC is limited access to fetal human tissues for experimental studies. Newly established techniques[17–19] creating enteroids from human intestine are a promising tool for the development of a patient-derived in vitro model.[20–22] Enteroids, which are primary cultures generated from intestinal epithelial stem cells, can be used to study the epithelial component of several chronic inflammatory diseases involving the intestinal mucosa.[17,23] In this study, our aim was to generate organoids across the fetal age spectrum to determine specific regulated differences in fetal intestinal development related to the onset of NEC. We compared gene expression of the fetal enteroids (FEnS) with gene expression from enterospheres that we generated from biopsy specimens of adult intestine (AEnS) obtained during clinically indicated endoscopies. Observations made by comparing early and late fetal enterospheres with adult enterospheres are described and the potential for this technique for further studies is discussed.

Materials and Methods

Derivation of FEnS and AEnS From Fetal Intestine

Human sample collection and procedures were approved by institutional review board protocols 1999P003833 (Brigham and Women's Hospital, Boston, MA) and 2016P000949 (Massachusetts General Hospital, Boston, MA) for the derivation of FEnS and AEnS, respectively. Based on these institutional review board–approved protocols, we have pledged not to share the generated material (FEnS and AEnS).

The isolation of intestinal epithelial cells was performed according to previously published protocols[17,24] with minor modifications.

For fetal enterospheres (FEnS), intestinal fragments were collected from aborted fetuses and cut into small pieces. For adult enterospheres (AEnS), 4 biopsy specimens were collected from the duodenum of patients undergoing upper endoscopy (esophagogastroduodenoscopy) for other clinical evaluations who also consented to participate in the study. Both fetal-derived intestinal fragments and biopsy specimens were washed once in cold phosphate-buffered saline (PBS) (ThermoFisher Scientific, Waltham, MA). PBS was replaced with a dissociation buffer containing PBS, penicillin/streptomycin, 1 mmol/L dithiothreitol (Sigma-Aldrich, St. Louis, MO), and 0.5 mmol/L EDTA (Sigma-Aldrich). Intestinal fragments were incubated at 4°C for 30 minutes and then vigorously shaken to promote epithelium dissociation from the basal membrane. This procedure was repeated at least 3 times to collect multiple fractions. Supernatants containing intestinal crypts were processed further and plated in Matrigel as described in previous research.[24] Stem cell media was prepared according to previously published methods with minor modifications.[19,25] Intestinal stem cell media composition was as follows: 500 mL Dulbecco's modified Eagle medium (DMEM)/F12 11330-032, 5 mL penicillin/streptomycin 15140122, 5 mL nonessential amino acids 11140-050, 5 mL sodium pyruvate 11360-070, 5 mL N-2 17502, and 10 mL B-27 17504044 (all purchased from ThermoFisher Scientific); 50 mL fetal bovine serum F4135, 1 mmol/L acetylcysteine A9165, and 10 nmol/L gastrin G9145

§Authors share co-senior authorship.

Abbreviations used in this paper: **AD, adult duodenal; AEnS, adult-derived enterospheres; CLDN, claudin; ΔΔCT, relative threshold cycle; CXCL, chemokine (C-X-C motif) ligand; DMEM, Dulbecco's modified Eagle medium; EGF, epidermal growth factor; FDR, false discovery rate; FEnS, fetal-derived enterospheres; FITC, fluorescein isothiocyanate; HIO, human intestinal organoid; HS, *Escherichia coli* human commensal isolate; IFN, interferon; IL, interleukin; LPS, lipopolysaccharide A; MAMP, microbe-associated molecular pattern; NEC, necrotizing enterocolitis; NF-κB, nuclear factor-κB; PBS, phosphate-buffered saline; PCR, polymerase chain reaction; PGE2, prostaglandin E2; RPKM, reads per kilobase of transcript per million; RT-PCR, reverse-transcription polymerase chain reaction; TEER, transepithelial electrical resistance; TLR, Toll-like receptor; TNF, tumor necrosis factor; WAE, wound-associated epithelial cells.**

Most current article

2352-345X
https://doi.org/10.1016/j.jcmgh.2018.01.014

(all purchased from Sigma-Aldrich); 50 ng/mL epidermal growth factor (EGF) (AF-100-15; PeproTech, Rocky Hill, NJ). L-WRN mouse fibroblasts ATCC CRL-3276 conditioned media was prepared as previously described.[25] Stem cell media and L-WRN–derived conditioned media were combined in a 1:1 ratio (1:1 media), 500 nmol/L A-8301 SML0788-5MG (Sigma-Aldrich), 10 μmol/L Y27623 Y0503-5MG (Sigma-Aldrich), and 1 μmol/L PGE2 2296 (Tocris Bioscience, Avonmouth, Bristol, UK) were added before use.

By using the described protocol, we were able to isolate approximately 300 crypts per cm^2 of small intestine from biopsy or fetal aborted tissue. The viability of the crypts was greater than 90% in the described culturing conditions. Culture media was changed every other day. Derived enterospheres were passaged every 7–9 days using trypsin-based standard dissociation methods. The single cells were replated in Matrigel at approximately 2 million/mL to ensure a robust propagation of the organoids (replating efficiency: organoids per plated single cells, 1:100).

RNA Sequencing and Computational Analysis

RNA was extracted in TRIzol (ThermoFisher Scientific) according to the manufacturer's instructions. RNA was purified further using Direct-zol RNA Kits (ZYMO Research, Irvine, CA). Total RNA was subjected to polyA selection, followed by NGS library construction using the NEBNext Ultra Directional RNA Library Prep Kit for Illumina (New England Biolabs, Ipswich, MA). Sequencing was performed on an Illumina HiSeq 2500 instrument, and reads were mapped to the human reference genome (hg19 build) using STAR,[26] resulting in a range of 30–50 million aligned single-end 50-bp reads per sample. Read counts over transcripts were calculated using HTSeq v.0.6.0[27] based on the most current Ensembl annotation file for hg19. Functional annotation clustering was performed using DAVID v6.7.[28,29]

Gene ontology biological processes were represented using the REVIGO tool[30] (available: http://revigo.irb.hr/). Pathway analysis was performed using Kyoto Encyclopedia of Genes and Genomes (KEGG) mapper search pathway[31] (available: http://www.genome.jp/kegg/tool/map_pathway1.html).

Organoid-Derived Monolayer Generation

Cell monolayers were generated according to published protocols.[23] Single-cell suspensions derived from organoids were plated on Polyester (PET) membrane Transwell inserts with a 0.4-μm pore size (Corning Life Sciences, Corning, NY) at 1.0^6 cells/mL. The media was changed every other day. When the culture reached confluence, based on transepithelial electrical resistance (TEER) monitoring and microscope direct observation (approximately 10 days), the culture was apically treated with 5 μmol/L N-[(3,5-Difluorophenyl)acetyl]-L-alanyl-2-phenyl]glycine-1, 1-dimethylethyl ester (DAPT) in DMEM/F12 for 48 hours as previously described[23] to promote cell differentiation. All inhibitors were removed from 1:1 media on the basolateral side. In some experiments, monolayers were treated with *Escherichia coli*–derived lipopolysaccharide A 0111:B4 L4391 (Sigma-Aldrich) at 50 or 250 μg/mL for 4 hours before collecting supernatants (both apical and basolateral) and cell monolayers in TRIzol for cytokine secretion and for relative gene expression assessments, respectively.

TEER Measurements

Monolayer intestinal integrity and permeability were assessed with a dual planar electrode instrument (Endohm Evom; World Precision Instruments, Sarasota, FL) following the manufacturer's instructions. TEER values were monitored every day for a total of 10–11 days during monolayer development. Data are expressed as resistance per square centimeter (Ω/cm^2).

Transepithelial (Apical to Basolateral) Passage of Macromolecular Biomarker Tracers

Paracellular permeability was assessed by measuring the flux of fluorescein isothiocyanate (FITC)-dextran, with a molecular weight of 4.0 kilodaltons (Sigma-Aldrich), as previously described.[32]

Quantitative Reverse-Transcription Polymerase Chain Reaction

RNA was extracted in TRIzol, further purified using a Direct-zol RNA Kit, and retrotranscribed using a maxima H-minus first-strand complementary DNA synthesis kit (ThermoFisher Scientific) according to the manufacturer's instructions. The CFX96 real-time polymerase chain reaction (PCR) detection system (Qiagen, Venio, NL) was used for gene expression analysis. The oligonucleotide primers used for gene expression analysis are listed in Table 1 and were designed by the Massachusetts General Hospital primer bank (Boston, MA) and generated by Integrative Device Technology (San Jose, CA). The relative threshold cycle ($\Delta\Delta$CT) method[33] was used for assessing gene expression relative to the 18S housekeeping reference gene.

Transmission Electron Microscopy

Cell monolayers were fixed for 2 hours in 2% glutaraldehyde in 0.1 mol/L sodium cacodylate buffer, pH 7.4 (Electron Microscopy Sciences, Hatfield, PA), on Transwell membrane supports and then rinsed in 0.1 mol/L sodium cacodylate buffer. Specimens were postfixed with 1% osmium tetroxide for 1 hour at room temperature, rinsed again in 0.1 mol/L sodium cacodylate buffer, dehydrated through a graded series of 100% ethanol concentrations, dehydrated briefly in 100% propylene oxide, and pre-infiltrated overnight in a 1:1 mix of eponate resin (Ted Pella, Inc, Redding, CA) and propylene oxide. The following day, specimens were infiltrated in 100% eponate resin, embedded in flat molds with 100% eponate, and allowed to polymerize overnight at 60°C. Thin (70-nm) sections were cut using a Leica (Leica Biosystems, Wetzlar, Germany) EM UC7 ultramicrotome, collected onto formvar-coated grids, stained with uranyl acetate and lead citrate, and examined on a JEOL (Peabody, MA) JEM 1011 transmission electron microscope at 80 kV. Images were collected using an Advanced Microscopy Techniques digital imaging system (Advanced Microscopy Techniques, Woburn, MA).

Cytokine Measurements

Supernatants from both apical and basolateral sides of the monolayers were collected to determine a panel of

Table 1. Primers for Quantitative RT-PCR Analysis

Gene	Forward	Reverse
OLFM4	ACTGTCCGAATTGACATCATGG	TTCTGAGCTTCCACCAAAACTC
MUC6	FCTGCCCTATACCAGCAATGGA	CTGACCCATGTACTTCCGCTC
LYZ	CTTGTCCTCCTTTCTGTTACGG	CCCCTGTAGCCATCCATTCC
LCN2	GACAACCAATTCCAGGGGAAG	GCATACATCTTTTGCGGGTCT
IL22RA1	CCGGCTAACCCTGGAAGAC	TCCAAGGTGCATTTGGTAGGT
IL2RG	GTGCAGCCACTATCTATTCTCTG	GTGAAGTGTTAGGTTCTCTGGAG
IL6R	CCCCTCAGCAATGTTGTTTGT	CTCCGGGACTGCTAACTGG
IL12RB2	AGGACGAGACACCCACTTATAC	ATTGACAGCAGTAACCTTGGC
IL1R1	ATGAAATTGATGTTCGTCCCTGT	ACCACGCAATAGTAATGTCCTG
IL18	TCTTCATTGACCAAGGAAATCGG	TCCGGGGTGCATTATCTCTAC
IL10RA	CCTCCGTCTGTGTGGTTTGAA	CACTGCGGTAAGGTCATAGGA
SOCS3	CCTGCGCCTCAAGACCTTC	GTCACTGCGCTCCAGTAGAA
CLDN6	TGTTCGGCTTGCTGGTCTAC	CGGGGATTAGCGTCAGGAC
JAM3	CGGCTGCCTGACTTCTTCC	TGGGGTTCGATTGCTGGATTT
IRAKM	CAGCCAGTCTGAGGTTATGTTT	TTGGGAACCAACTTTCTTCAC
SI	TCCAGCTACTACTCGTGTGAC	CCCTCTGTTGGGAATTGTTCTG
IL8	ACTGAGAGTGATTGAGAGTGG	AACCCTCTGCACCCAGTTTTC
TNF	CCTCTCTCTAATCAGCCCTCTG	GAGGACCTGGGAGTAGATGAG
LGR5	PPH13346A Qiagen	
CLDN4	CGGCCCACAACATCATCCAA	GGCGGAGTAAGGCTTGTCT
PTGER4	CATCATCTGCGCCATGAGTGT	GCTTGTCCACGTAGTGGCT
18S	AGAAACGGCTACCACATCCA	CCCTCCAATGGATCCTCGTT

proinflammatory cytokines, including interferon-γ (IFN-γ), interleukin (IL)1β, chemokine (C-X-C motif) ligand (CXCL)8, tumor necrosis factor (TNF), and IL6, using a Mesoscale (Rockville, MD) U 9-plex (K15067L-1) according to the manufacturer's directions. Cytokines were analyzed with MSD Discovery Workbench 4.0 software (Rockville, MD).

Immunofluorescence Staining

Monolayers and enteroids were fixed in 4% paraformaldehyde embedded in paraffin, sectioned, and directly stained according to standard procedures, as previously described.[34] The following antibodies were used: anti-mucin2, Sc-15334 (Santa Cruz Biotechnology, Santa Cruz, CA), dilution 1:200; anti-TJP1, 339100 (ThermoFisher Scientific), dilution 1:100; anti-villin, 610359 (BD Biosciences, San Jose, CA), dilution 1:50; anti-sucrase isomaltase, Sc-27603 (Santa Cruz Biotechnology), dilution 1:200; and anti–epithelial cell adhesion molecule, MA5-12436 (Life Technologies, MA), dilution 1:100. Ulex europaeus agglutinin 1 conjugated with FITC (ulex europaeus agglutinin 1–FITC) was used to detect M-cells (bright)[35] and enterocytes (low)[36] (50 μg/mL) (Sigma-Aldrich). 4'-6'-diamino-2phenylindole (Sigma-Aldrich), was used for nuclei counterstaining at 1 μg/mL. The images were acquired using an Eclipse confocal microscope (Nikon, Melville, NY) and composed using Adobe Photoshop CS6 software.

In Situ Hybridization of Intestinal Tissue

RNAscope LS 2.5 Probe Hs-OLFM4, 311041 Peptidyl-prolyl Isomerase B probe, 313901-positive control were purchased from Advanced Cell Diagnostic (Newark, CA). In situ hybridization experiments were performed according to the manufacturer's protocol and as previously described.[34] Images were acquired using a Nikon Eclipse microscope 80i and composed using Adobe Photoshop CS6 software.

Western Blot Analysis

Experiments were performed according to standard procedures and as previously described.[34] The following antibodies were used: anti-P65 (L8F6) mouse monoclonal antibody, 6956, dilution 1:1000; anti-NFKB Inhibitor Alpha (L35A5) mouse monoclonal antibody, 4814 at 1:1000 (Cell Signaling Technology, Danvers, MA); and anti–β-actin rabbit monoclonal antibody, 926-42210 at 1:1000 (LI-COR Biosciences, Lincoln, NE). Western blot images were acquired using a LI-COR Odyssey scanner. Protein band densitometry analysis was performed using LI-COR Image Studio version 5.2 software.

Escherichia coli *Human Commensal Isolate Strain Commensal Bacteria Growth and Experimental Treatment Procedure of Monolayers*

HS *E coli* was grown and heat killed as previously described,[32,37] with the following modifications. HS was cultured in Luria broth with shaking overnight. The next day the culture was diluted 1:200 and grown for 2 hours (0.5 optical density). The culture was resuspended in DMEM/F12 before being heat-killed by boiling for 10 minutes. The culture was diluted further to a final multiplicity of infection bacteria/epithelial cells of 100:1, and added to cell monolayers for 4 hours.

Table 2. Scraped Mucosae Data Set for Figure 4*A*

Sample	Description	Source	Donor ID	Accession number
HuSI.Duo.A1	Adult duodenum	EMBL-EBI array express	V145	E-MTAB-1733 (duodenum_4a)
HuSI.Duo.A2	Adult duodenum	EMBL-EBI array express	V150	E-MTAB-1733 (duodenum_4b)
HuSI.F91	Fetal, small intestine, gestational age 91 days (13 wk)	GEO data sets	H-23914	GSM1059508
HuSI.F98	Fetal, small intestine, gestational age 91 days (14 wk)	GEO data sets	H-23964	GSM1059508
HuSI.F108	Fetal, small intestine, gestational age 91 days (15.5 wk)	GEO data sets	H23769	GSM1059521
HuSI.F115	Fetal, small intestine, gestational age 91 days (16.5 wk)	GEO data sets	H-23808	GSM1059517
HuSI.F120	Fetal, small intestine, gestational age 91 days (17 wk)	GEO data sets	H-29941	GSM1059519

Accession Numbers

RNA-sequencing data generated for this study were uploaded at NCBI-GEO databank, accession number: GSE101531 (https://www.ncbi.nlm.nih.gov/geo/query/acc.cgi?acc=GSE101531). Other data set accession numbers used for comparison and previously published are listed in Table 2.

Statistical Analysis

Differential expression analysis of RNA-sequencing data was performed using the EdgeR package (version 3.8.6),[38] based on the criteria of more than 2-fold change in expression value and false discovery rates (FDRs) (Benjamini–Hochberg) $< .05$ and a hypergeometric enrichment test.

All other statistical analyses were performed using the *t* test or ordinary 1-way analysis of variance using GraphPad Prism (La Jolla, CA) 7.01 as stated in the text.

All authors had access to the data and have reviewed and approved the final manuscript.

Results

Generation of a Human-Derived FEnS Repository

We derived enterospheres (FEnS) from the small intestines of 6 aborted fetuses, ranging in gestational age from 11 to 22.5 weeks (Table 3), based on previously developed protocols for human organoid cultures.[17,19,24,39] Five of 6 FEnS were generated from the duodenum; FEnS 11 (F11) was derived from the whole small intestine. Applying identical procedures, we derived 3 (AD11, AD14, and AD 15) enterospheres (AEnS) from adult duodenal biopsy specimens (Table 3).

We evaluated the growth factor requirement for the generated FEnS cultures (Figure 1*A*). As previously reported,[19,40] we found that both EGF and wingless-type MMTV integration site family gene signaling are indispensable in supporting the growth of human FEnS. Accordingly, the adopted culture media contained factors wingless-type MMTV integration site family gene 3A, R-spondin 1, and noggin, provided as conditioned media,[25] recombinant EGF, and prostaglandin E2 (PGE2).[19]

Although PGE2 is necessary for FEnS,[19] it is not required for the maintenance of duodenum-derived AEnS.[24] PGE2 has been shown to promote the differentiation of wound-associated epithelial cells (WAE) over enterocytes.[41] However, by promoting cell differentiation, we were able to up-regulate the expression of sucrase isomaltase, an enterocyte-specific gene,[42] in both AEnS and FEnS (Figure 1*B*). The relative abundance of WAE cells under different culture conditions was evaluated in AEnS by the expression of Prostaglandin E2 receptor 4 (PTGER4) and claudin 4 (CLDN4), WAE-specific markers[41,43] (Figure 1*C* and *D*). In line with previous observations, both PTGER4 and CLDN4 were found to be up-regulated in adult duodenal-derived enteroids cultured with PGE2, although the finding was not statistically significant for both markers. Immunofluorescence

Table 3. FEnS and AEnS Sample Sets of Human Enteroid Samples

ID	Description	Procedure	Sex	Age, *y*	IRB
F11	Organoids derived from 11-week gestational age intestine	Abort	N/A	N/A	1999P003833
F14	Organoids derived from 14-week gestational age duodenum	Abort	N/A	N/A	1999P003833
F15	Organoids derived from 15-week gestational age duodenum	Abort	N/A	N/A	1999P003833
F17.5	Organoids derived from ~17.5-week gestational age duodenum	Abort	N/A	N/A	1999P003833
F21.5	Organoids derived from ~21-week gestational age duodenum	Abort	N/A	N/A	1999P003833
F22.5	Organoids derived from ~22-week gestational age duodenum	Abort	N/A	N/A	1999P003833
AD11	Organoids derived from adult healthy volunteer duodenum	EGD	F	58	2016P000949
AD14	Organoids derived from adult healthy volunteer duodenum	EGD	F	52	2016P000949
AD15	Organoids derived from adult healthy volunteer duodenum	EGD	F	59	2016P000949

EGD, esophagogastroduodenoscopy.

staining with the anti–epithelial cell adhesion molecule epithelial pan marker[44] and the antivillin endodermal marker[45] (Figure 1*E*–*G*) were used to validate the intestinal epithelial origin of FEnS (Figure 1*E* and *F*) and AEnS (Figure 1*G*). Nonetheless, based on our decision to minimally manipulate the cultures, we could not exclude that a small percentage of other cell types were co-purified during the generation of both FEnS and AEnS.

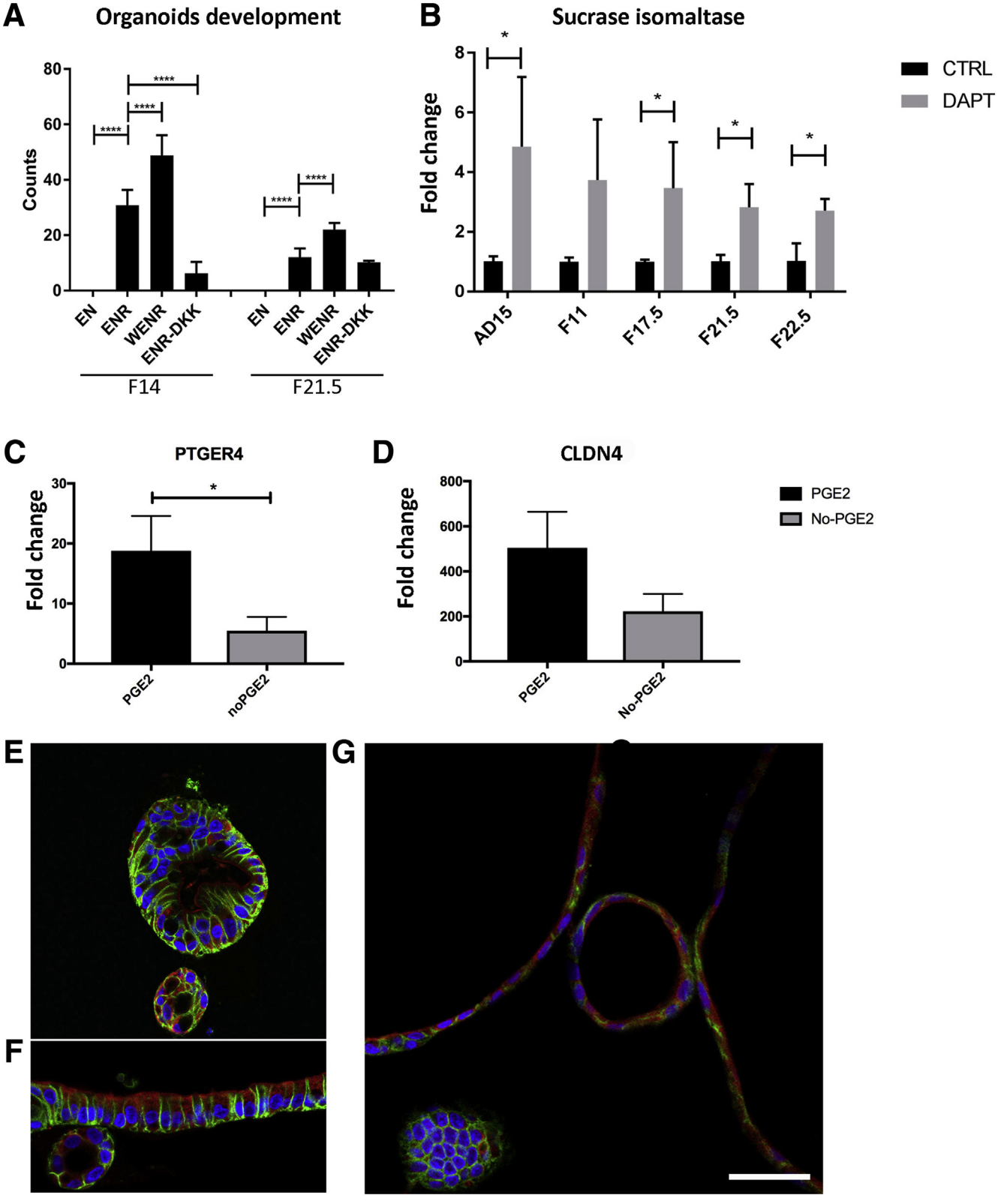

RNA-Sequencing Analysis Comparison Showed Significant Differences Between FEnS and AEnS Gene Expression

We sought to compare the global gene expression profile of FEnS and AEnS by RNA-sequencing analysis. We evaluated FEnS (N = 6) and AEnS (N = 3) samples at a low passage, ranging from P6 to P14. Genes were considered expressed if their respective reads per kilobase of transcript per million (RPKM) mapped read values were $\geq$1.0 (Supplementary Worksheet 1). Differential expression analysis produced 844 genes whose expression was significantly different between the 2 sample groups (Supplementary Worksheet 2). The levels of expression (RPKM) for these genes are shown as a heatmap in Figure 2*A*. AEnS and FEnS samples clustered into 2 main groups (Figure 2*A*). All FEnS shared a third-tier clade with AEnS samples. Samples F14 and F15 (named hereafter *early FEnS*) clustered together and shared a second-tier clade with a second group of FEnS including F11 and F17.5, F21.5, and F22.5 (named *late FEnS*).

Late FEnS appeared to group between early FEnS and AEnS (Figure 3*A*), suggesting an intermediate gene expression profile. F11 behaved as an outlier for a subgroup of genes and consequently clustered with the late FEnS (Figures 2*A* and 3*A*). We performed differential gene expression analysis between AEnS and the identified FEnS subgroups (fold-change, 2; FDR $\leq$ 0.5). We found that 1909 genes were differentially regulated between AEnS and early FEnS, whereas 679 genes were differentially expressed between AEnS and late FEnS. Finally, 1255 genes were expressed differentially between early FEnS and late FEnS (Figure 3*C* and Supplementary Worksheets 2–4). We used the DAVID functional annotation tool to perform gene set enrichment analysis of up-regulated genes in AEnS compared with all FEnS (fold-change $>$ 2; FDR $<$ 0.05) (Figure 2*B* and Supplementary Worksheet 5). Consistent with previous data from fetal intestinal mucosae,[46] we observed that the most significantly represented terms were associated with relevant functions of the intestinal epithelium, including cellular response to cytokine stimuli, defense response, epithelium development, and cell proliferation (Figure 2*B*).

Fetal Enterospheres Recapitulate Fetal Intestinal Development

Our gene analysis suggested that fetal enterospheres clustered in groups based on the developmental age of their respective tissue of origin, therefore we hypothesized that late FEnS might represent the fetal intestinal epithelium of a later gestational age (specifically 17.5–22.5 wk) and closely resemble the intestinal epithelium of a viable premature infant at higher risk of developing NEC. We generated supervised heatmaps representing the expression of the genes associated with 3 relevant biological functions critical for NEC pathogenesis: epithelium differentiation, innate immunity, and the tight junction network (Figure 2*C*–*E*).

As hypothesized, gene expression levels of late FEnS clustered alternately with the early FEnS or AEnS or showed intermediate levels between the other 2 groups, and thus were not always significantly different from either group (Figure 2*C*–*E* and Table 4). F11 did not behave as an outlier for most of the analyzed gene subsets but was similar to the early FEnS (Figure 2*C*–*E*). The expression of a subset of genes was validated by quantitative reverse-transcription PCR (RT-PCR), confirming the RNA-sequencing data set (Figure 3*D*). Epithelial cell maturation markers were found to be up-regulated significantly in AEnS compared with early FEnS (Figure 2*C* and Table 4). Conversely, the expression of the stem cell marker LGR5 was higher in early FEnS than in AEnS, a finding that concurred with previous reports.[19,46] Interestingly, OLFM4 and LYZ were expressed at low levels in early FEnS and up-regulated in late FEnS, similar to AEnS (Figure 2*C* and Table 4).

In line with a maturing immune system, we observed a significant up-regulation of many chemokines, including CXCL8/IL8, and cytokine receptors IL10RA (an important mediator of immune tolerance[47]) and IL1R1, and IgA receptor polymeric immunoglobulin receptor in AEnS compared with early FEnS (Figure 2*D* and Table 4).

Late FEnS expressed, in a manner similar to AEnS, significantly high levels of CXCL8/IL8. Nonetheless, IL10RA receptor was up-regulated in AEnS but not in late FEnS (Figure 2*D* and Table 4). TLR4 and TLR2, previously reported to be up-regulated in fetal intestine,[15] were only slightly, but not significantly, up-regulated in early FEnS.

Figure 1. (***See previous page***). **Establishing human FEnS repository.** (*A*) Growth of F14 and F21.5 enterospheres was evaluated in different media conditions to establish a minimum growth factor requirement. The same number of cells (50,000/mL) were seeded. Enteroids were counted after 5 days of culture. Standard DMEM/F12 media was supplemented with N2, B27, acetyl cysteine, gastrin, and PGE2 (see the Materials and Methods section for more detail), and the following were supplemented as labeled in the figure: E, EGF (50 ng/mL); N, noggin (100 ng/mL); W, wingless-type MMTV integration site family gene (WNT) 3A (100 ng/mL); R, R-spo1 (1 μg/mL); and DKK, Dickkopf-related protein-1, WNT inhibitor (50 ng/mL). Multiple comparison analysis was performed adopting the 1-way analysis of variance test: ****$P < .0001$. (*B*) AEnS and FEnS were cultured in standard growing media or by adding 5 μmol/L N-[(3,5-Difluorophenyl)acetyl]-L-alanyl-2-phenyl]glycine-1,1-dimethylethyl ester in DMEM/F12 for 48 hours to promote cell differentiation. Sucrase isomaltase gene expression was evaluated for monitoring enterocyte differentiation. The ΔΔCT method was used to calculate fold-change in quantitative PCR analysis (*t* test, *$P < .05$). (*C*) Gene expression of PTGER4 and (*D*) CLDN4 was evaluated by quantitative RT-PCR in adult duodenum-derived enterospheres (AD11, AD14, and AD15) cultured with or without PGE2. Fold-change refers to gene expression in no-PGE2 samples and was calculated by applying the ΔΔCT method. *Bar* indicates SD (*t* test, *$P < .05$). (*E*) Immunofluorescence staining was performed on human enterospheres cultured for 5 days and identified, respectively, as follows: F15, from 15 weeks' fetal duodenum; (*F*) F21.5, from 21.5 weeks' fetal duodenum; (*G*) AD15, from adult duodenum biopsy specimens. Enterospheres were stained with 4'-6'-diamino-2phenylindole nuclear marker (blue), the epithelial pan marker epithelial cell adhesion molecule (green), and the intestinal specific marker villin 1 (red) to validate their derivation from the small intestinal epithelial cells of the gut. *Scale bar*: 100 μm. Culturing conditions, efficiency of generation, and efficiency in replating are described in the Materials and Methods section. CTRL, control.

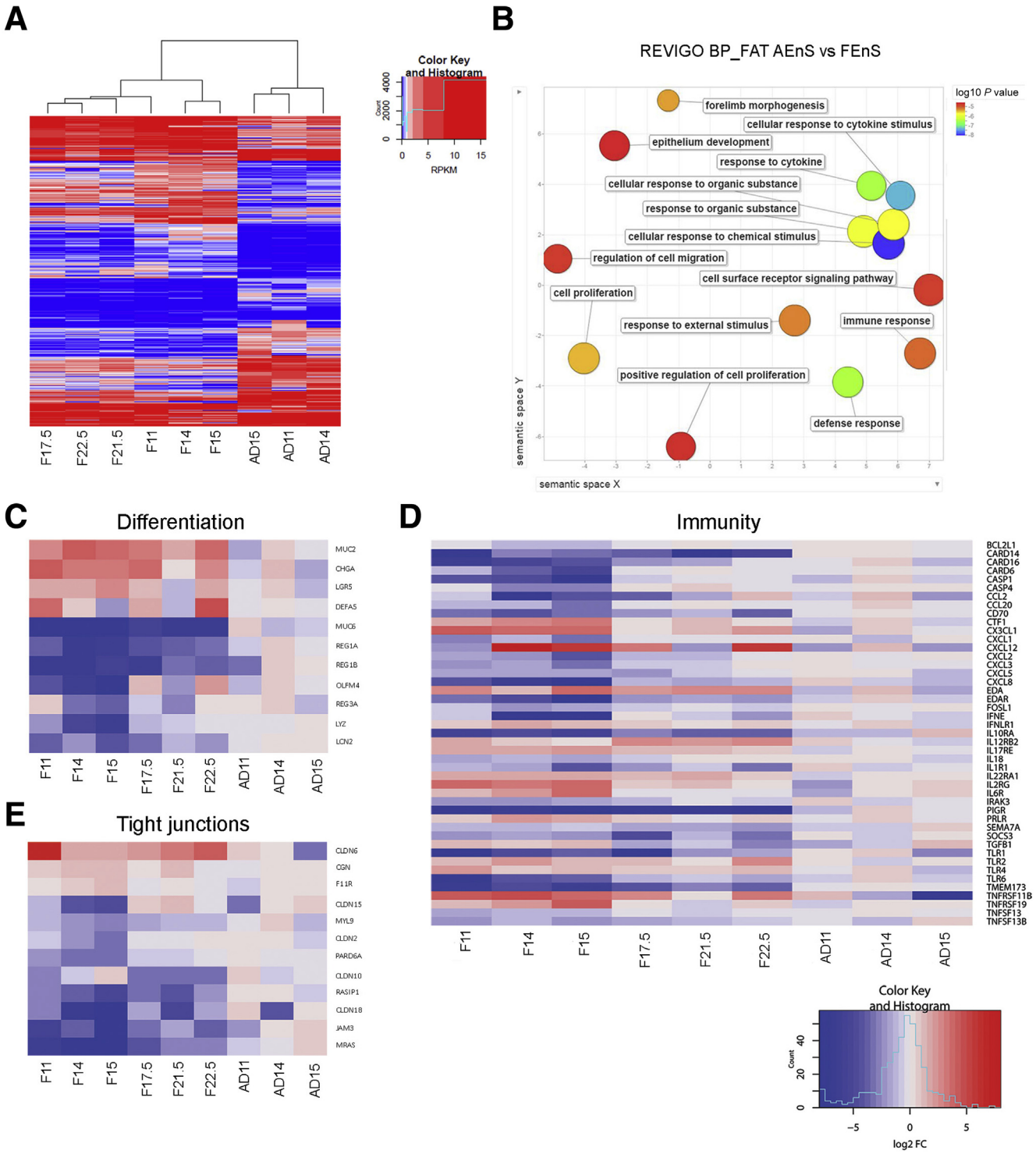

Figure 2. Analysis of gene expression in FEnS and AEnS. (*A*) Heatmap of RPKM values for expressed genes, with hierarchal clustering of samples. Expression values are indicated by color, from blue (low) to red (high). (*B*) Reduce and Visualize Gene Ontology representation of Gene Ontology of Biological Processes (Biological Processes_Functional annotation tool) analysis performed on significantly up-regulated genes between AEnS and all FEnS groups (FDR $< .05$). The diagram summarizes the enriched gene categories grouped by functional annotations and represented as $\log_{10}$ *P* value (enrichment > 1.5) as *colored circles*. The semantic similarity measure used was SimRel. (*C*) Heatmap representing the expression of genes from functional categories associated with epithelial differentiation, (*D*) immunity, and (*E*) tight junctions that were found differentially expressed between early FEnS and AEnS. The selected genes were identified based on GO BP_FAT terms, KEGG database (Supplementary Worksheet 7), or direct data set analyses and were considered relevant to NEC pathogenesis. Gene expression is represented as $\log_2$ (fold-change) compared with the average expression in AEnS samples. The color key code is at the bottom right of figure (Supplementary Worksheet 8).

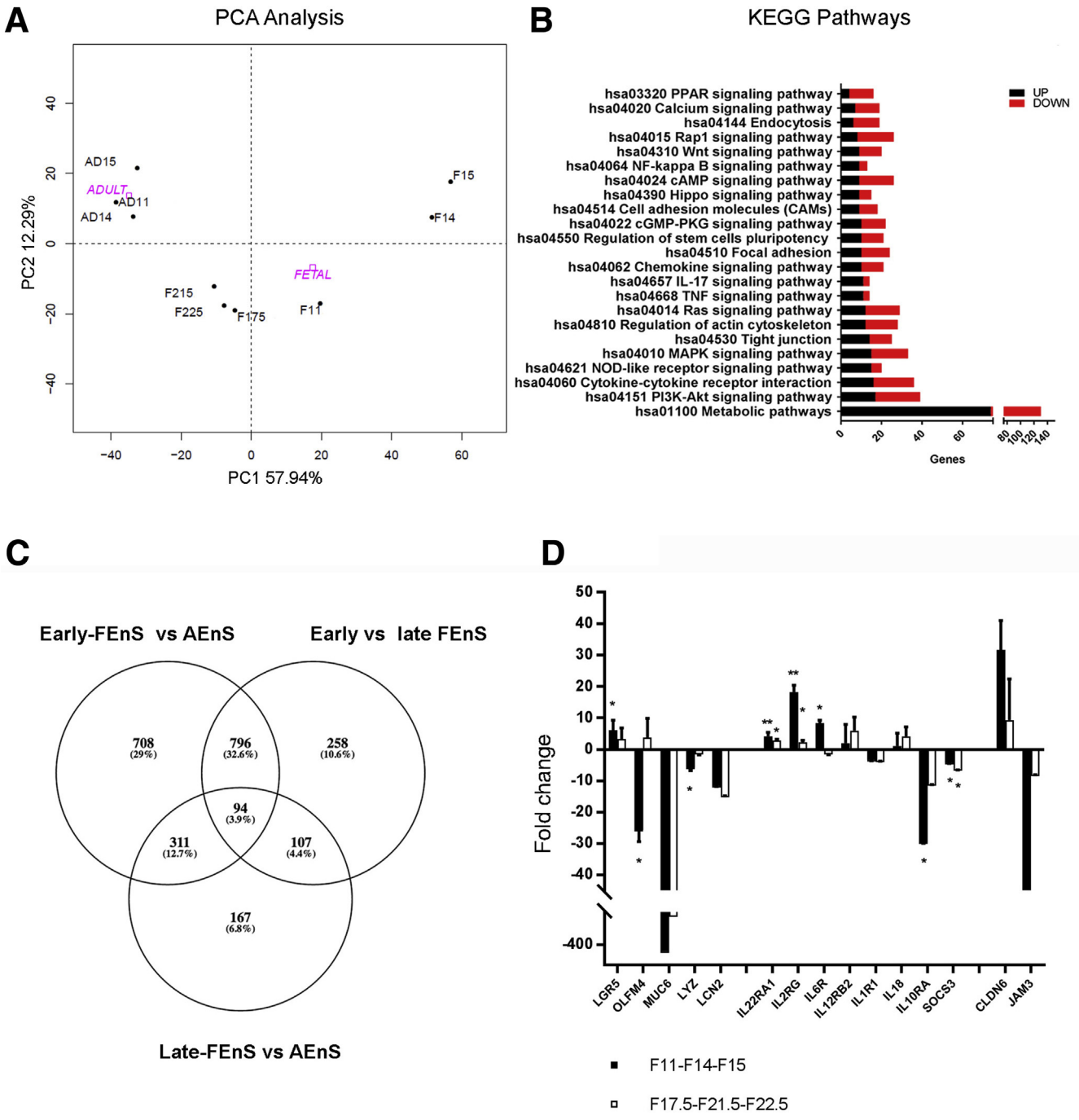

Figure 3. Identification of FEnS subgroups, pathways analysis, and quantitative RT-PCR validation of RNA-sequencing data. (*A*) Principal component analysis (PCA) loading plot showing grouping of samples based on gene expression patterns among differentially expressed genes. The top 2 components (PC1 and PC2) account for 68.2% of the variation in the data set. *Pink squares* indicate the average position for AEnS and FEnS sample sets, respectively. (*B*) Selected pathways enriched in genes with increased (black) and decreased (red) expression, identified by KEGG database between the early FEnS and the AEnS (fold-change $>$ 2; FDR $<$ .05) data sets. (*C*) Venn diagrams represent overlapping of gene sets that are differentially expressed among a subgroup of samples identified as early FEnS (F14 and F15), late FEnS (F17.5, F21.5, and F22.5), and AEnS (AD11, AD14, and AD15) based on PCA analysis (panel *A*) and hierarchical clustering samples represented in Figure 2*A*. (*D*) Quantitative RT-PCR analysis to validate selected genes found to be differentially regulated among early FEnS, late FEnS, and AEnS by RNA-sequencing and belonging to relevant functional groups: cell differentiation, immunity, and tight junctions. Fold-change (ΔΔCT) was calculated relative to AEnS (baseline). *Bar* indicates SD. One-way analysis of variance test: $^{*}P < .05$, $^{**}P < .01$.

Table 4. FDR of Supervised Differentially Expressed Genes Associated With Differentiation Processes, Innate Immunity, and Tight Junctions (Figure 2*C–E*)

	AEnS vs early FEnS	AEnS vs late FEnS	AEnS vs All FEnS
Differentiation			
LYZ	1.42667E-27	0.323819784	0.294860266
DEFA5	0.964649685	0.058391039	0.182401261
REG3A	0.001966287	1	0.993697162
OLFM4	9.73592E-06	0.880064166	1
MUC2	2.03933E-09	1.73207E-05	3.69072E-06
MUC6	6.65946E-22	1.24839E-17	1.78115E-14
CHGA	0.000189769	0.003855845	0.000309997
LGR5	0.001806323	0.480984026	0.052721986
REG1A	1.16426E-25	3.26159E-15	3.77122E-11
REG1B	2.5681E-05	0.001376676	4.14476E-06
LCN2	1.49369E-05	0.000520059	1.73525E-06
Immunity			
BCL2L1	0.003554024	1	0.656999445
CARD14	0.016776555	4.93254E-06	0.000156316
CARD16	0.000247657	0.590799819	0.153751025
CARD6	7.88686E-10	1	0.843344069
CASP1	2.2153E-07	1	0.636934155
CASP4	1.66143E-08	1	0.998091144
CCL2	0.029937929	1	0.981821753
CCL20	0.004908219	1	0.825620999
CD70	1.16943E-05	0.009303721	5.6947E-05
CTF1	0.010133791	#N/A	0.329390641
CX3CL1	1.96967E-05	0.443601741	0.024966336
CXCL1	0.022976196	1	0.614259854
CXCL12	9.1169E-05	0.050116509	0.070806633
CXCL2	0.0017659	0.713752456	0.149772735
CXCL3	0.000446371	0.953391228	0.215491056
CXCL5	0.03633074	0.606094846	0.077607785
CXCL8	1.67503E-15	0.10804406	0.100608195
EDA	0.003154097	0.045776149	0.01467591
EDAR	3.68396E-06	0.047212333	0.007111427
FOSL1	1.19941E-06	0.527507924	0.183638093
IFNE	0.000375571	1	0.789550444
IFNLR1	0.013765775	0.834265959	0.290402307
IL10RA	0.001121616	0.011136533	5.37206E-05
IL12RB2	#N/A	0.00070892	0.085364188
IL17RE	3.46592E-05	0.044957767	0.002822468
IL18	0.00485898	1	0.820500762
IL1R1	0.042544119	0.230030263	0.040208655
IL22RA1	0.000428558	0.024168451	0.003645441
IL2RG	6.83543E-08	0.742139183	0.017469909
IL6R	8.22758E-05	1	0.366280071
IRAK3/IRAKM	0.028405452	0.831309045	0.200687261
PIGR	3.28354E-16	8.5372E-23	1.22405E-45
PRLR	0.002619569	1	0.327790619
SEMA7A	0.298194793	0.015534844	0.035970325
SOCS3	0.11964226	0.027823392	0.00613506
TGFB1	0.459951339	0.117590039	1
TLR1	0.035380942	0.227880366	0.022177122
TLR2	0.081425452	0.171613486	0.123214442
TLR4	0.357988148	0.754004589	0.317321154
TLR6	0.002643264	0.676151717	0.181212641
TMEM173	3.194E-11	3.10524E-07	4.60837E-08
TNFRSF11B	0.000868963	0.160632711	0.020424457
TNFRSF19	1.50336E-08	1	0.087079785
TNFSF13	0.198658596	1	0.686177148
TNFSF13B	0.162487642	0.473521594	0.094583569
Tight junctions			
CLDN18	3.90784E-05	0.252671508	0.056147135
CLDN2	8.3306E-08	1	0.757001124
CLDN15	3.20047E-05	1	1
CLDN10	0.9264975	9.5884E-05	0.702989844
CLDN6	0.070424985	0.00020942	0.007059523
PARD6A	6.50513E-06	0.901477971	0.285393036
MRAS	7.77881E-07	0.003884293	0.000435292
RASIP1	1.1531E-05	0.000167959	2.13299E-06

Table 4. Continued

	AEnS vs early FEnS	AEnS vs late FEnS	AEnS vs All FEnS
JAM3	0.001818244	0.057749814	0.001931379
F11R	0.047768944	1	0.80233348
CGN	0.011095209	0.643381723	0.158667149
MYL9	0.006903959	0.297115858	0.065833081

However, Interleukin 1 Receptor Associated Kinase 3 (IRAK3/IRAKM) and Suppressor Of Cytokine Signaling 3, negative regulators of, respectively, TLR4 receptor signaling[48] and the janus kinase/Signal Transducer And Activator Of Transcription pathway[49] (Figure 2*D* and Table 4), were significantly up-regulated in AEnS only. Genes belonging to the Nucleotide Binding Oligomerization Domain Containing 2-like pathway, including Caspase Recruitment Domain Family Member 6, which is essential in NF-κB activation,[50] were transcriptionally up-regulated in AEnS and late FEnS compared with early FEnS (Figure 2*D* and Table 4).

Finally, we evaluated the expression of tight junction network genes. In line with previous observations in fetal intestine, CLDN6[51] was greatly up-regulated in FEnS (Figure 2*E* and Table 4) compared with AEnS. We found that CLDN18, CLDN2, CLDN15, and junctional adhesion molecule 3 all were up-regulated significantly in both late FEnS and AEnS (Figure 2*E* and Table 4).

To further corroborate our observations, we also compared genes differentially expressed between AEnS and FEnS with published data from the scraped mucosae of human adult and fetal intestine. Because FEnS and AEnS

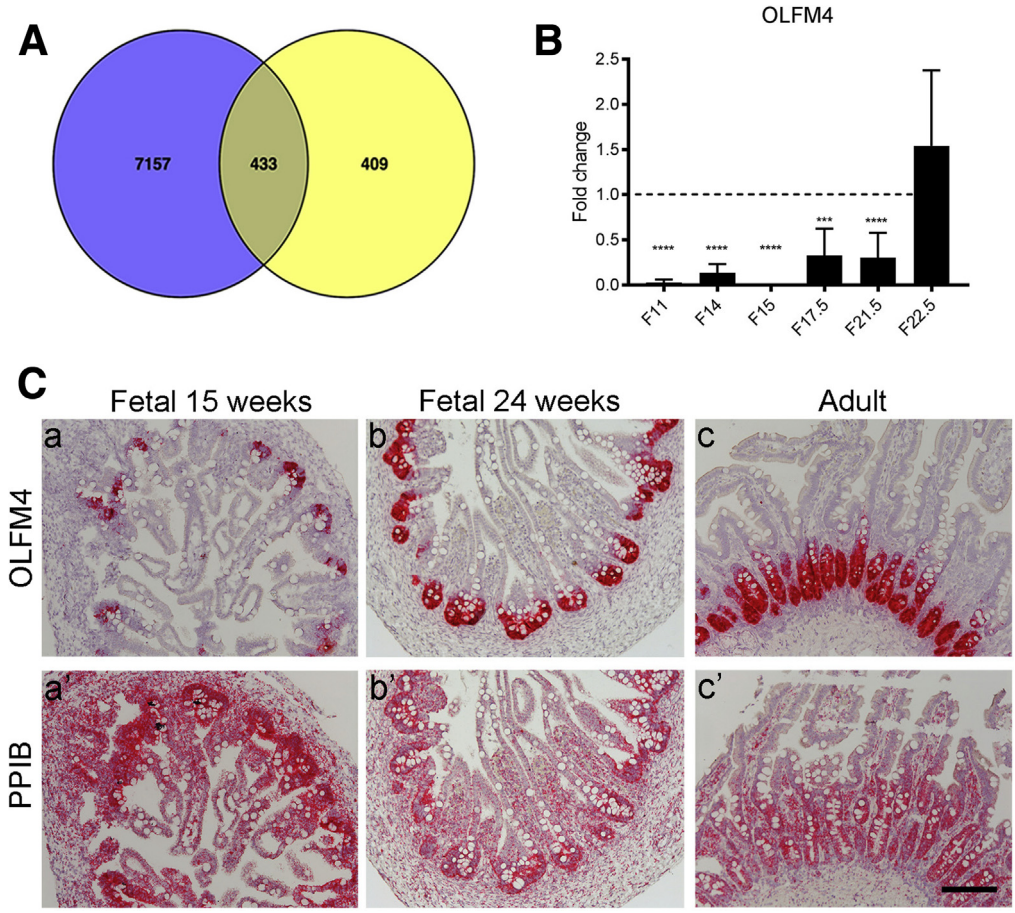

Figure 4. Functional gene set enrichment analysis. (*A*) Venn diagram summarizing the overlap of gene sets differentially expressed between AEnS and FEnS (fold change > 2). (FDR < .05) compared with differentially expressed genes (fold-change > 2) in human intestinal mucosa from adult and fetal origin. No FDR cut-off value was applied to the scraped mucosae sample sets. Significant overlap was calculated using the hypergeometric test ($P < 3.567e\text{-}159$). (*B*) Gene expression of OLFM4 was assessed by quantitative RT-PCR analysis in FEnS compared with AEnS (*dotted line*) and is expressed as fold-change. Multiple comparison analysis was calculated using the 1-way analysis of variance test: ***$P < .001$, ****$P < .0001$ (Dunnett multiple comparison test). (*C*) In situ hybridization of OLFM4 and positive control Peptidylprolyl Isomerase B was performed on human intestinal tissue from 15 weeks' and 24 weeks' gestational age and adults. Positive control ensured comparable staining intensity across the sample sets. *Scale bar*: 200 μm.

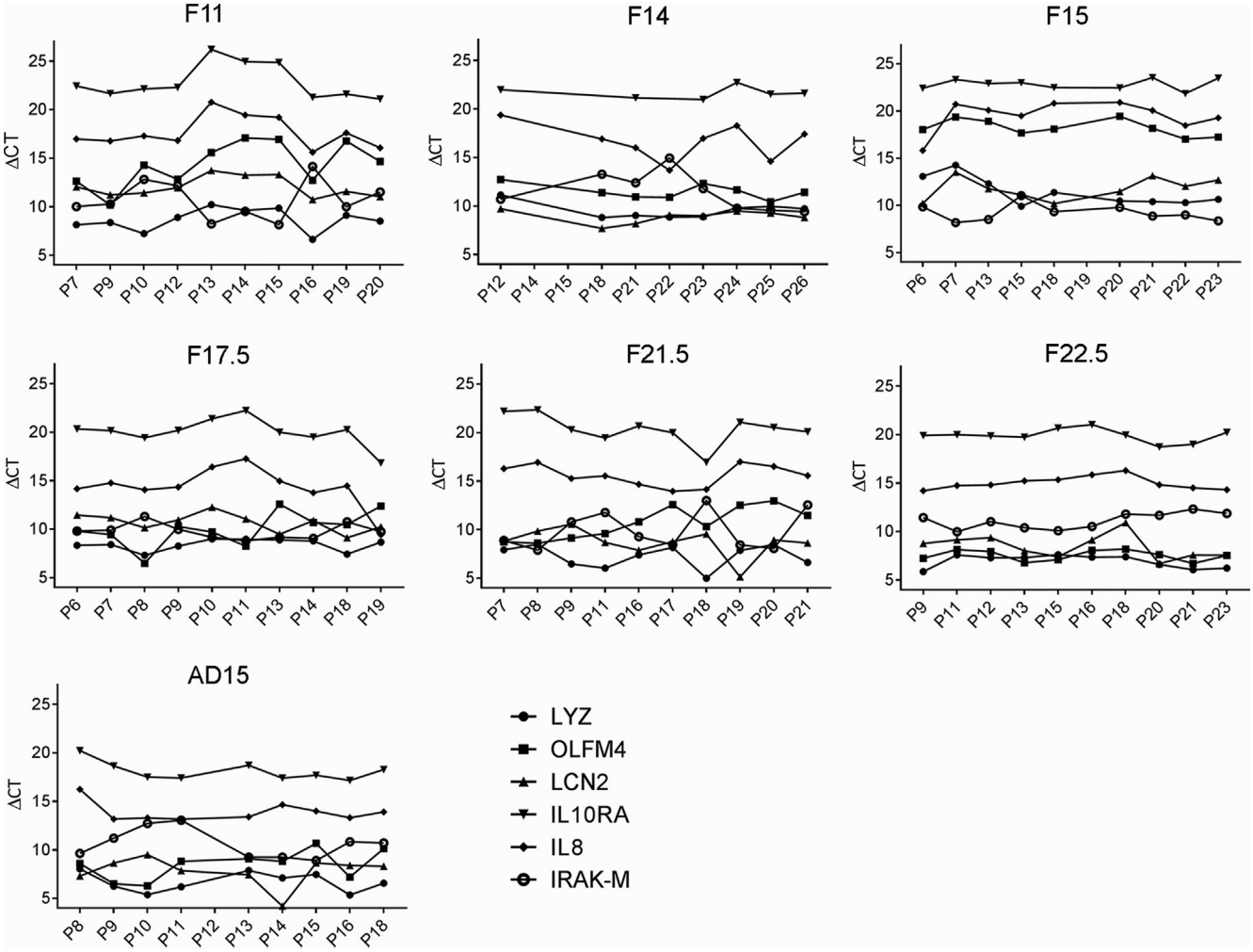

Figure 5. Expression over time of selected developmentally regulated genes in FEnS and AEnS. The expression of LYZ, OLFM4, LCN2, IL10RA, IL8/CXCL8, and IRAKM was assessed by quantitative RT-PCR analysis in the sample sets over approximately 15 passages. ΔCT represents the relative expression of the gene of interest and was calculated by subtracting the CT value of the housekeeping gene 18S from the CT of each investigated gene. The ΔCT values were plotted against the relative passage for each of the 6 genes and are represented as connected lines in the graphs; each graph represents 1 sample. Straight lines connecting the ΔCT values were interpreted as a stable expression of the analyzed genes over multiple passages. The legend indicates the symbol assigned to each gene.

exclusively represent the epithelial component, whereas scraped mucosae may include immune and lamina propria cells, we focused on the expression of genes that were detected (RPKM $>$ 1) in our data set. A total of 433 genes, representing 50% of differentially regulated genes between FEnS and AEnS, were similarly regulated in both sample sets (Figure 4*A* and Supplementary Worksheet 6), with a highly significant overlap in the gene set enrichment analysis ($P <$ 3.567e-159).

Finally, we analyzed in greater detail the expression of the gene OLFM4, an intestinal stem cell marker.[52] OLFM4 was previously found to be significantly less expressed in fetal intestine compared with adult.[46] In line with this observation we found that *OLFM4* was significantly down-regulated in early FEnS (Figure 2*C*). Quantitative RT-PCR analysis further confirmed a significant down-regulation of OLFM4 in all FEnS, except F22.5, when compared with AEnS (Figure 4*B*). Because OLFM4 expression directly correlated with the developmental age of the tissue of origin of the FEnS (Figures 2*C* and 4*B*), we hypothesized that OLFM4 could be up-regulated during fetal intestinal development. To test our hypothesis, we performed messenger RNA in situ hybridization of OLFM4 in the intestinal mucosae from adults and fetuses at multiple gestational ages (Figure 4*C*). In line with our genetic data in FEnS, we found that OLFM4 was less expressed in fetal intestinal mucosae at 15 weeks compared with adult intestine, but it was considerably up-regulated in tissue derived from fetuses at 24 weeks' gestational age (Figure 4*C*).

FEnS and AEnS Express a Stable Transcriptome Over Time

Gene expression stability has been hypothesized to be a challenge for induced pluripotent stem cell–derived cell lines.[53] Furthermore, fetal-derived spheres from mouse intestine have been shown to transition into an adult

phenotype under specific culture conditions.[19] To evaluate the AEnS and FEnS transcriptomes over time, we subcultured the enterospheres weekly (every 7–9 days), collected samples for approximately 15 passages, representative of roughly 4 months, and analyzed them by quantitative RT-PCR. We evaluated the expression of selected genes that previously had been found differentially expressed in fetal- and adult-derived enterospheres, including LYZ, OLFM4, LCN2, IL10RA, CXCL8/IL8, and IRAKM (Figure 5), by plotting the gene ΔCT values over multiple passages. We found that over the studied timeline and passages, the expression of these genes remained relatively stable over time for all the samples tested (Figure 5).

Late FEnS Monolayers Respond to E coli *and Lipopolysaccharide Stimulation*

Based on our observation that innate immunity–related pathways were developmentally regulated in our samples of enterospheres, we strove to establish the capacity of the early and late FEnS to respond to bacteria. To test our hypothesis, we generated monolayers from both AEnS and FEnS as previously reported.[23] Both AEnS and FEnS developed polarized monolayers with apical microvilli, tight junctions (Figure 6*A* and *B*), and desmosomes (Figure 6*A*). The monolayers also developed both secretory and absorptive cell populations as shown by immunofluorescence staining for ulex europaeus agglutinin 1 and mucin2 markers (Figure 6*B* and *C*). TEER showed similar time kinetics for all monolayers, which plateaued in 5–8 days (Figure 6*D*). The evaluation of neutral molecule passage, such as dextran–FITC (Figure 6*E*), suggested a functional barrier in AEnS-, F21.5-, and F22.5-derived monolayers, whereas younger FEnS (F14, F15, and F17.5) were significantly leaky despite a similar TEER. Overall, FEnS showed a different capacity for sealing the paracellular space that inversely correlated with the respective developmental age of the tissue of origin (Figure 6*E*).

We assessed the ability of the monolayers to respond to a human commensal *E coli* bacteria strain (HS).[54] The

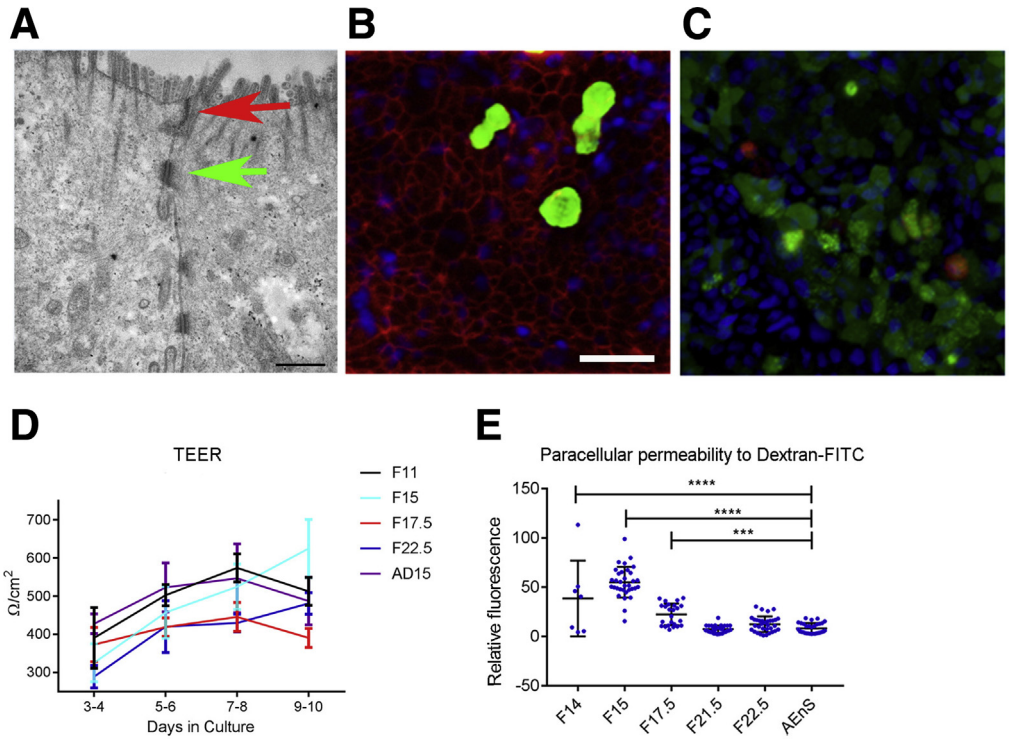

Figure 6. FEnS monolayer development and characterization. (*A*) Transmitted electron microscopy of F11-derived monolayer showed the presence of polarized enterocytes with developed microvilli. Tight junctions (*red arrow*) and desmosomes (*green arrow*) also were observed sealing the paracellular space. *Scale bar*: 0.2 μm. (*B*) Immunofluorescence staining F22.5-derived monolayer with anti-tight junction protein1/zonula occludens 1 (*red*) and anti-mucin2 (*green*) showed the presence of tight junctions and goblet cells, respectively. (*C*) Immunofluorescence staining of F22.5-derived monolayer using ulex europaeus agglutinin 1–FITC (*green*) and antibody directed against sucrase isomaltase (red) identified the presence of, respectively, immature enterocytes (ulex europaeus agglutinin–positive low), M-cells (ulex europaeus agglutinin–positive high), and mature enterocytes (sucrose isomaltase positive); 4'-6'-diamino-2phenylindole (*blue*) was used for nuclei counterstaining. *Scale bar*: 100 μm. (*D*) Time course of TEER measurement to assess monolayer development of FEnS (F11, F15, F17.5, and F22.5) and AD15 (representative for AEnS). Experiments were repeated at least 3 times in triplicate. Averages and SDs are reported. (*E*) Paracellular permeability measured in FEnS and AEnS (AD15) by 4-kilodalton dextran–FITC passage in the basolateral side after 4 hours of incubation. The fluorescence reads were normalized vs the apical dextran–FITC pool and were represented as arbitrary units. Experiments were repeated at least 3 times in triplicate. Averages and SDs are reported. Multiple comparison analysis was performed with 1-way analysis of the variance: ***$P < .001$; ****$P < .0001$ (Dunnett multiple comparison test).

development of cell monolayers was monitored by daily TEER reads. When 2 consecutive measurements showed unchanged TEER, we promoted the cell monolayer differentiation as previously reported.[18,23,55] We opted to challenge the monolayers with HS heat-killed bacteria to test the ability of the monolayers to respond to a wide range of bacteria microbe-associated molecular patterns (MAMPs) and to preserve the monolayer viability.[32] Both FEnS and AEnS responded to the HS challenge based on the transcriptional activation of proinflammatory cytokines TNF and CXCL8/IL8 (Figure 7*A* and *B*). However, response from younger FEnS (F11, F15, and F17.5) was modest and not significant, whereas more mature F21.5 and F22.5 mounted a significant reaction, comparable with AEnS. No changes in the viability of cells across the samples was detected by lactate dehydrogenase assay (data not shown). As predicted by the RNA-sequencing analysis (Figures 2*B* and *D*, and 3*B*), we hypothesized that early FEnS might be less responsive toward MAMPs because they do not yet have fully active immune response machinery in place. To test our hypothesis, we further investigated the level of the P65 part of the NF-κB complex and its negative regulator NFKB Inhibitor Alpha. We observed that early FEnS expressed lower levels of P65 protein, whereas no significant differences were observed between late FEnS and AEnS (Figure 7*C* and *D*). NFKB Inhibitor Alpha-negative regulator was expressed at comparable levels across all of the samples (Figure 7*C*).

Because TLR4 activation has been previously hypothesized to be relevant in the immune response of an immature intestine to colonizing bacteria and in relationship to NEC development,[11,14,15] we further investigated the contribution of purified lipopolysaccharide (LPS) to the observed bacteria response. LPS challenge did not alter TEER or passage of dextran–FITC and did not affect monolayer viability (data not shown). A significantly increased expression of TNF and CXCL8/IL8 was detected in LPS-treated monolayers derived from F21.5 and F22.5 only, whereas no significant up-regulation of either cytokine was observed in early FEnS or AEnS (Figure 8*A* and *B*) monolayers. Finally, we evaluated the secretion of

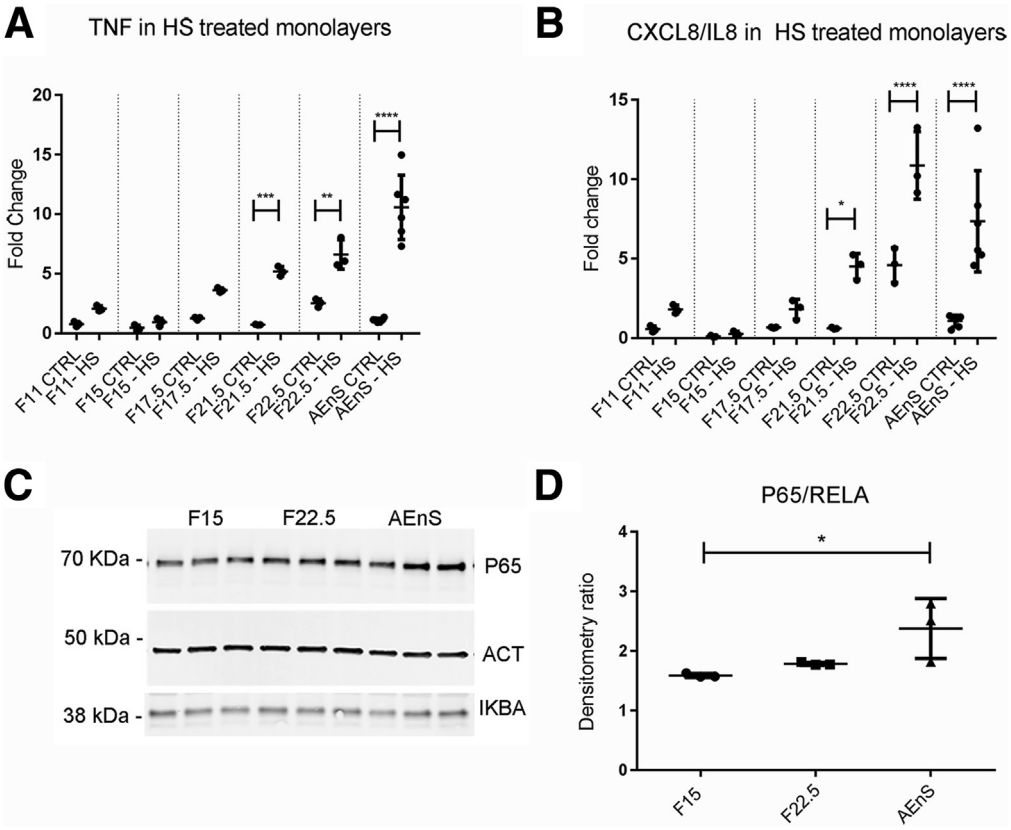

Figure 7. Proinflammatory cytokine profiles in HS heat-killed bacteria-treated monolayers and NF-κB pathway assessment. (*A*) TNF and (*B*) CXCL8/IL8 gene expression were evaluated in HS heat-killed treated and untreated monolayers for 4 hours at a multiplicity of infection of 100:1. Fold-change was calculated based on expression levels of TNF or CXCL8/IL8 in AEnS control represented by AD14, using the ΔΔCT method. Multiple comparison analysis was performed applying 1-way analysis of variance comparing each HS-treated sample with its respective control (analysis of variance, Sidak multiple comparison test) $^{*}P < .05$, $^{**}P < .01$, $^{***}P < .001$, and $^{****}P < .0001$. (*C*) Baseline protein levels of P65 and NFKB Inhibitor Alpha were established in triplicate samples of F15, F22.5, and AEnS (represented by AD14) total protein extracts. (*D*) Densitometric analysis of P65 compared with actin (ACT) internal control of the Western blot shown in panel *C* is expressed as a ratio and was calculated using Image Studio Lite Ver 5.2 (LI-COR). Statistical analysis was performed using 1-way analysis of variance: $^{*}P < .05$ (Dunnett multiple comparison test).

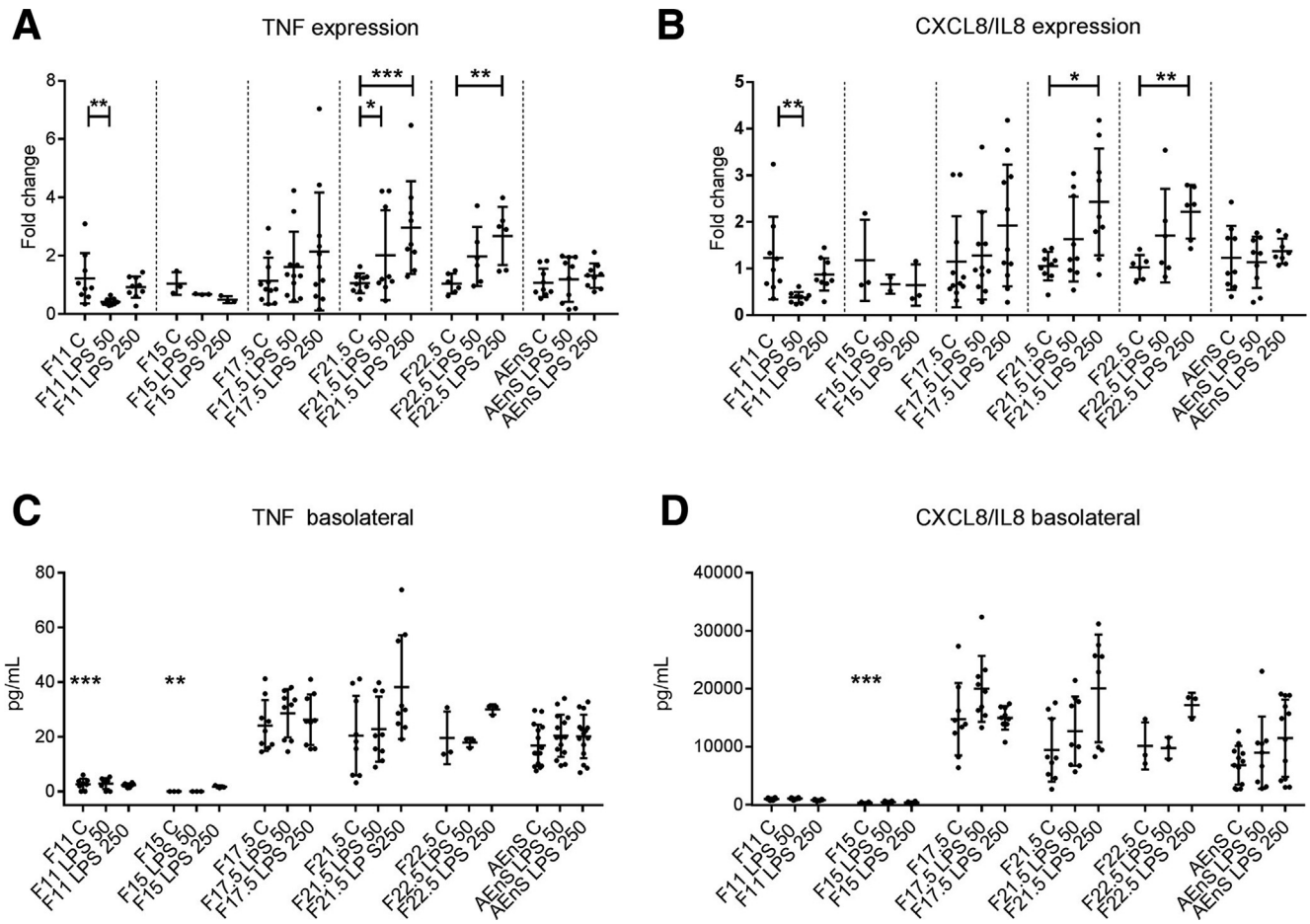

Figure 8. Cytokine assessment in LPS-treated monolayers. (*A*) TNF and (*B*) CXCL8/IL8 expressions were assessed in monolayers treated with 2 concentrations of LPS (50 and 250 μg/mL) labeled as LPS 50 and LPS 250, respectively. The gene expression was compared with AEnS (AD15) control and represented as the fold-change. Statistical analysis was performed using a nonparametric Wilcoxon paired rank test to compare each control with respective LPS-treated samples. (*C*) TNF and (*D*) CXCL8/IL8 cytokines were assessed in the basolateral supernatants of FEnS and AEnS LPS-treated monolayers. Cytokine secretion differences among all FEnS controls and AEnS control were evaluated by the Kruskal–Wallis test. $^{*}P = .05$, $^{**}P < .05$, and $^{***}P < .01$.

proinflammatory cytokines including TNF, CXCL8/IL8, IFN-γ, IL6, and IL1β, after LPS challenge. Cytokines were measured in both apical and basolateral compartments and showed a similar trend. Only basolateral cytokine measurements are shown (Figure 8*C* and *D*). At baseline, early FEnS, represented by F11 and F15, secreted barely detectable cytokines that were significantly lower when compared with AEnS (Figure 8*C* and *D*). In unstimulated monolayers, late FEnS and AEnS had comparable levels of cytokines (Figure 8*C* and *D*). The LPS challenge moderately, but not significantly, increased the release of TNF and CXCL8 in F21.5 and F22.5 at high dosage (Figure 8*C* and *D*). A similar trend was observed for IFN-γ secretion, which was increased in the basolateral and apical culture media of F21.5 and F22.5 upon treatment with high doses of LPS (Figure 9), but not in AEnS or early FEnS. No changes were observed in IL1β and IL6 secretion (data not shown).

Finally, we evaluated the effect of PGE2 on the response of AEnS monolayers to LPS stimuli (Figure 10). PGE2 increased the basal expression of IL8 and TNF (data not shown). However, it did not significantly change the modality of the response to LPS treatment in terms of TNF release. A significant reduction of IL8 and IFN-γ secretion was observed in monolayers not treated with PGE2 and exposed to higher doses of LPS only (Figure 10).

Discussion

Our study aimed to characterize the human fetal enterosphere as a suitable model to investigate intestinal development and to generate a novel intestinal ex vivo human epithelial model for the study of NEC. Having established multiple enterospheres from aborted fetuses across the fetal age spectrum, we have shown by RNA-sequencing analysis that enterospheres derived from fetal and adult human intestine retain a distinct and developmentally regulated gene expression program that correlates with their developmental age. Our observations were corroborated by the significant gene expression similarities between scraped mucosae from adult and fetal intestine and

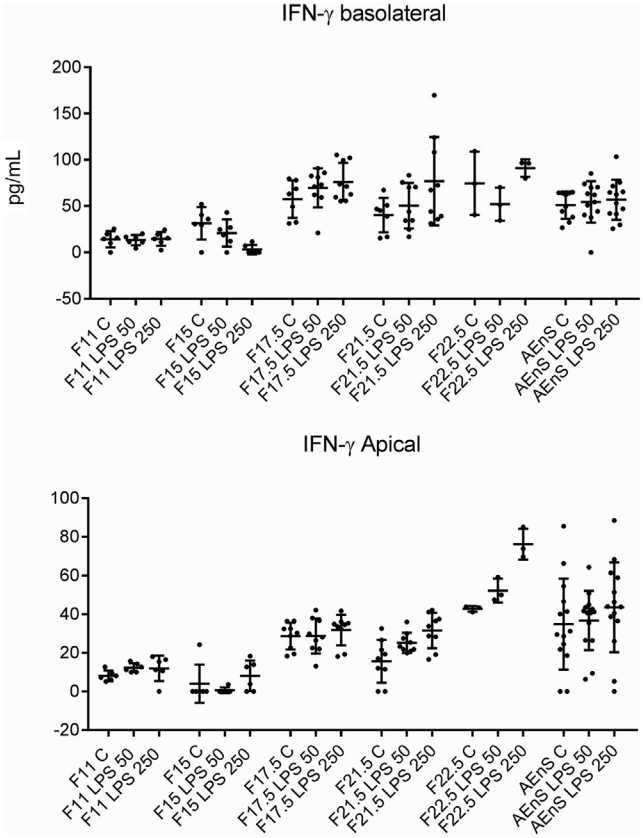

Figure 9. Apical and basolateral IFN-γ cytokine release. IFN-γ was evaluated in the experimental groups early FEnS (FEnS 11 and F15), late FEnS (FEnS 17.5, F21.5, and F22.5), and AEnS (AD15) in untreated (C) and 2 concentrations of LPS: 50 and 250 μg/mL, respectively.

enterospheres from adult and fetal origin. Furthermore, our observations are in accord with a recent study showing that enteroids from patients retain a gene expression program inherited from the respective tissue of origin.[56]

Consistent with previous gene expression analysis of fetal intestinal mucosae,[46] we observed that genes associated with the innate immune response, intestinal epithelium maturation, and gut barrier function were down-regulated significantly in FEnS compared with AEnS. However, we also observed more subtle gene expression changes occurring among the FEnS correlating with their developmental age. We found that a set of genes associated with Paneth cell antimicrobial activity[57,58] (LYZ and REG3A), stem cell function[52] (OLFM4), and the innate immune response (including inflammasome-related chemokines and cytokines, cytokine receptors, and TNF-related and CXCL8/IL8 genes) were up-regulated in a subgroup of FEnS derived from developmentally more mature fetuses, specifically from 17.5 to 22.5 weeks gestational age. Although the fetal-specific claudin-6,[51] part of the tight junction network, was highly expressed in all the FEnS but not in the AEnS, we uncovered other genes associated with regulation of paracellular permeability, including JAM3, claudin-2, and claudin-15, which were found to be significantly underexpressed in early FEnS compared with AEnS, but were up-regulated in late FEnS in a manner similar to AEnS. Consistent with the molecular data, we also reported that late FEnS (only F21.5 and F22.5) and adult-derived monolayers had comparable paracellular permeability, whereas monolayers from younger FEnS appeared significantly more permeable.

In contrast with the transcriptome instability reported for mouse-derived fetal enterospheres,[19] we did not observe substantial changes of the gene expression program in long-term passage (roughly 4 months), at least for a subgroup of genes that were developmentally regulated. These data suggest that FEnS of human origin are transcriptionally stable under the adopted culture conditions and appropriate for long-term use in a biorepository. Altogether, our data corroborate the hypothesis that fetal enterospheres recapitulate the gene expression of their tissue of origin and retain their developmentally regulated programs pertinent to their respective gestational age over time.

NEC pathology has been associated with the hyperactive immune response of the immature intestine to environmental stimuli, particularly bacteria and their bioproducts.[5]

In this study, we provide functional evidence of the ability of FEnS to elicit a proinflammatory response to MAMPs, which could recapitulate the in vivo response of an immature intestine. We used a heat-killed nonpathogenic *E coli* strain derived from a patient isolate (HS)[54] as a prototype for commensal bacteria. In line with the gene expression analysis, our observations suggested a significant activation of innate immunity in late FEnS and AEnS only. The low responsiveness of early FEnS correlated with significantly lower levels of P65 protein, a critical component of the NF-κB complex, compared with both late FEnS and AEnS.

Previous evidence has shown that in NEC as well as in fetal nondiseased tissue,[14] LPS-driven activation of the pattern recognition receptor TLR4 was instrumental in promoting inflammation via the NF-κB signaling pathway.[11,59] Furthermore, a mouse carrying an epithelium-specific TLR4 knockdown was protected from developing NEC.[60] The TLR4 receptor also was found to be up-regulated in fetal intestine compared with mature gut,[15] whereas its negative regulators were found to be down-regulated.[11]

Based on these data we further investigated the contribution of LPS to the immune response to the commensal *E coli* in FEnS and AEnS. Our observation showed that only late FEnS, but not AEnS or early FEnS, increased TNF and CXCL8/IL8 activation at the transcriptional level and increased, although not significantly, release of both cytokines upon LPS treatment.

Taken together, our data are consistent with previously published findings and support the hypothesis that TLR4 immune regulators capable of damping immune responses are functionally up-regulated only in adults, whereas only the fetal intestine from midgestational age (21.5–22.5 wk), but not younger or adults, is likely to activate a proinflammatory response mediated by the LPS–TLR4–NF-κB axis.

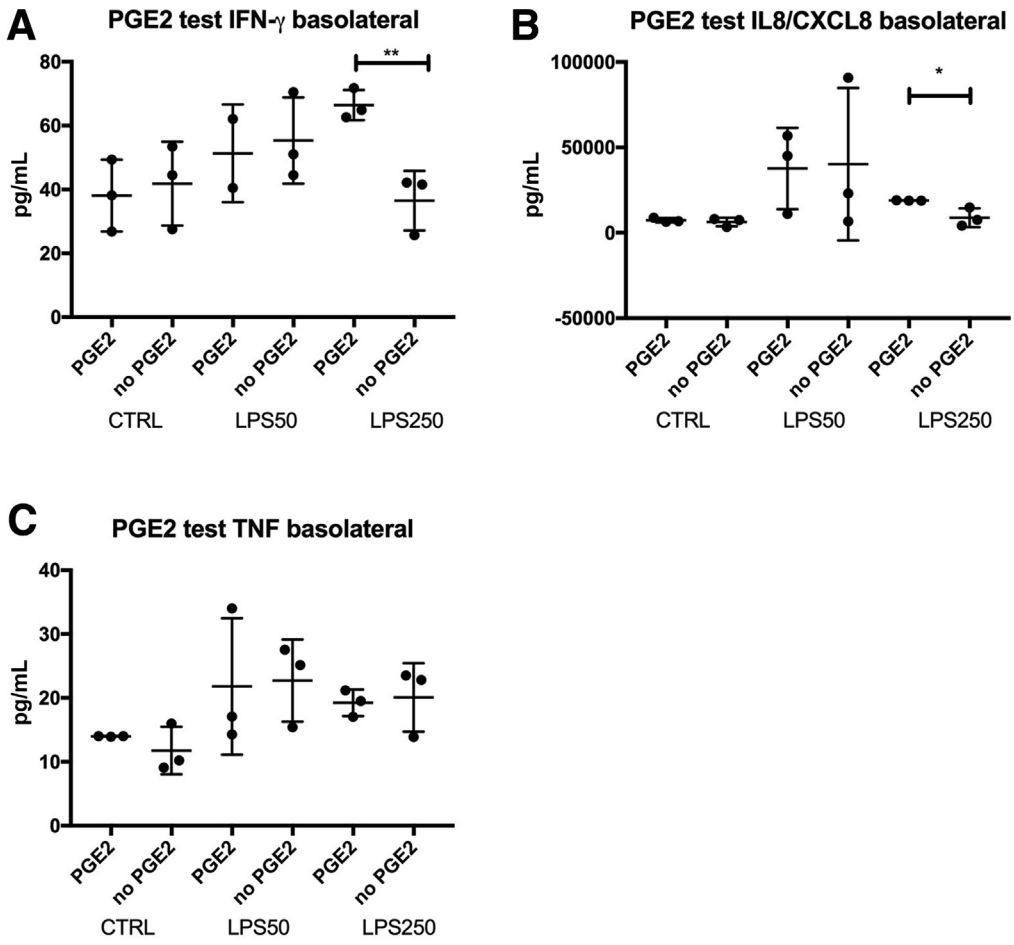

Figure 10. PGE2 effect on cytokine release in AEnS-derived monolayers. (*A*) IFN-γ, (*B*) IL8/CXCL8, and (*C*) TNF cytokine secretion was evaluated in AD11, representative of AEnS-derived monolayers cultured with or without PGE2, and challenged with LPS at 50 μg/mL (LPS50) and 250 μg/mL (LPS250). One-way analysis of variance: $^{*}P < .05$, $^{**}P < .01$. CTRL, control.

Culture conditions to generate and maintain human FEnS have been established previously,[19,39] and for study consistency were adopted for the entire sample sets including PGE2 as a supplement. PGE2 has been shown to promote the differentiation of WAE in adult intestine-derived enteroids instead of enterocytes.[41] In our culturing conditions, we observed up-regulation of the WAE markers PTGER4 and CLDN4 in AEnS. However, we were able to promote the differentiation of enterocytes as well, based on sucrose isomaltase gene up-regulation, by applying previously described media conditions.[23] Moreover, in our functional assay, PGE2 did not substantially affect TNF and CXCL8/IL8 release after LPS treatment in AEnS, suggesting that PGE2 did not alter the interpretation of our functional data.

Based on our evidence, we propose that late FEnS represent a valid model to study NEC pathogenesis and could complement other human-derived models used for the same purpose, with a few advantages. The use of xenografts of human fetal intestine currently is considered one of the most valuable models to recapitulate intestinal and relative innate immunity maturation, which are both thought to play an important role in NEC pathophysiology.[61] However, the xenograft model requires long-term growth in a mouse host, has a low rate of grafting owing to tissue-limited availability, and allows only for a single experiment set. Conversely, the FEnS model can be frozen and resuscitated, and in a manner similar to a cell line, it can be used for multiple experiments, providing virtually unlimited tissue access. More recently, the development and characterization of human intestinal organoids (HIO) from induced pluripotent stem cell[46] has been proposed as a suitable model for NEC. Gene expression analysis has shown that HIO resembles fetal intestinal tissue rather than adult.[46] Upon transplantation in a mouse host, HIO can achieve a certain degree of maturation because a robust increase of OLFM4 was reported.[46] As with FEnS, HIO offers similar advantages to a cell line, however, similar to the xenograft model, HIO might require implantation into a host to promote maturation. Consequently, HIO could be subject to a higher variability in experimental procedures associated with the host-implant compared with in vitro experiments performed using FEnS.

We plan to extend these observations to include enterospheres established from NEC tissue at the time of surgical resection for the disease. This technique could help to determine the enterosphere's response, which may predispose the immature intestine to the expression of the conditions of NEC. By determining these mechanisms of NEC inflammation, we may be able to devise strategies to prevent its expression.

References

1. Stoll BJ, Hansen NI, Bell EF, Walsh MC, Carlo WA, Shankaran S, Laptook AR, Sanchez PJ, Van Meurs KP, Wyckoff M, Das A, Hale EC, Ball MB, Newman NS, Schibler K, Poindexter BB, Kennedy KA, Cotten CM, Watterberg KL, D'Angio CT, DeMauro SB, Truog WE, Devaskar U, Higgins RD. Eunice Kennedy Shriver National Institute of Child Health and Human Development Neonatal Research Network. Trends in care practices, morbidity, and mortality of extremely preterm neonates, 1993-2012. JAMA 2015;314:1039–1051.
2. Rowe MI, Reblock KK, Kurkchubasche AG, Healey PJ. Necrotizing enterocolitis in the extremely low birth weight infant. J Pediatr Surg 1994;29:987–991.
3. Glass HC, Costarino AT, Stayer SA, Brett CM, Cladis F, Davis PJ. Outcomes for extremely premature infants. Anesth Analg 2015;120:1337–1351.
4. Huda S, Chaudhery S, Ibrahim H, Pramanik A. Neonatal necrotizing enterocolitis: clinical challenges, pathophysiology and management. Pathophysiology 2014; 21:3–112.
5. Neu J, Walker WA. Necrotizing enterocolitis. N Engl J Med 2011;364:255–264.
6. Herrmann K, Carroll K. An exclusively human milk diet reduces necrotizing enterocolitis. Breastfeed Med 2014; 9:184–190.
7. Savidge TC, Morey AL, Ferguson DJ, Fleming KA, Shmakov AN, Phillips AD. Human intestinal development in a severe-combined immunodeficient xenograft model. Differentiation 1995;58:361–371.
8. Sangild PT, Ney DM, Sigalet DL, Vegge A, Burrin D. Animal models of gastrointestinal and liver diseases. Animal models of infant short bowel syndrome: translational relevance and challenges. Am J Physiol Gastrointest Liver Physiol 2014;307:G1147–G1168.
9. Sanderson IR, Ezzell RM, Kedinger M, Erlanger M, Xu ZX, Pringault E, Leon-Robine S, Louvard D, Walker WA. Human fetal enterocytes in vitro: modulation of the phenotype by extracellular matrix. Proc Natl Acad Sci U S A 1996;93:7717–7722.
10. Clark DA, Mitchell AL. Development of gastrointestinal function: risk factors for necrotizing enterocolitis. J Pediatr Pharmacol Ther 2004;9:96–103.
11. Nanthakumar N, Meng D, Goldstein AM, Zhu W, Lu L, Uauy R, Llanos A, Claud EC, Walker WA. The mechanism of excessive intestinal inflammation in necrotizing enterocolitis: an immature innate immune response. PLoS One 2011;6:e17776.
12. Nanthakumar NN, Fusunyan RD, Sanderson I, Walker WA. Inflammation in the developing human intestine: a possible pathophysiologic contribution to necrotizing enterocolitis. Proc Natl Acad Sci U S A 2000; 97:6043–6048.
13. Claud EC, Lu L, Anton PM, Savidge T, Walker WA, Cherayil BJ. Developmentally regulated IkappaB expression in intestinal epithelium and susceptibility to flagellin-induced inflammation. Proc Natl Acad Sci U S A 2004;101:7404–7408.
14. Afrazi A, Sodhi CP, Richardson W, Neal M, Good M, Siggers R, Hackam DJ. New insights into the pathogenesis and treatment of necrotizing enterocolitis: Toll-like receptors and beyond. Pediatr Res 2011; 69:183–188.
15. Meng D, Zhu W, Shi HN, Lu L, Wijendran V, Xu W, Walker WA. Toll-like receptor-4 in human and mouse colonic epithelium is developmentally regulated: a possible role in necrotizing enterocolitis. Pediatr Res 2015;77:416–424.
16. Cahill CM, Zhu W, Oziolor E, Yang YJ, Tam B, Rajanala S, Rogers JT, Walker WA. Differential expression of the activator protein 1 transcription factor regulates interleukin-1ss induction of interleukin 6 in the developing enterocyte. PLoS One 2016;11:e0145184.
17. Jung P, Sato T, Merlos-Suarez A, Barriga FM, Iglesias M, Rossell D, Auer H, Gallardo M, Blasco MA, Sancho E, Clevers H, Batlle E. Isolation and in vitro expansion of human colonic stem cells. Nat Med 2011;17:1225–1227.
18. Sato T, Stange DE, Ferrante M, Vries RG, Van Es JH, Van den Brink S, Van Houdt WJ, Pronk A, Van Gorp J, Siersema PD, Clevers H. Long-term expansion of epithelial organoids from human colon, adenoma, adenocarcinoma, and Barrett's epithelium. Gastroenterology 2011;141:1762–1772.
19. Fordham RP, Yui S, Hannan NR, Soendergaard C, Madgwick A, Schweiger PJ, Nielsen OH, Vallier L, Pedersen RA, Nakamura T, Watanabe M, Jensen KB. Transplantation of expanded fetal intestinal progenitors contributes to colon regeneration after injury. Cell Stem Cell 2013;13:734–744.
20. Schweiger PJ, Jensen KB. Modeling human disease using organotypic cultures. Curr Opin Cell Biol 2016; 43:22–29.
21. Grant CN, Grikscheit TC. Tissue engineering: a promising therapeutic approach to necrotizing enterocolitis. Semin Pediatr Surg 2013;22:112–116.
22. Aurora M, Spence JR. hPSC-derived lung and intestinal organoids as models of human fetal tissue. Dev Biol 2016;420:230–238.
23. VanDussen KL, Marinshaw JM, Shaikh N, Miyoshi H, Moon C, Tarr PI, Ciorba MA, Stappenbeck TS. Development of an enhanced human gastrointestinal epithelial culture system to facilitate patient-based assays. Gut 2015;64:911–920.
24. Sato T, Vries RG, Snippert HJ, van de Wetering M, Barker N, Stange DE, van Es JH, Abo A, Kujala P, Peters PJ, Clevers H. Single Lgr5 stem cells build crypt-villus structures in vitro without a mesenchymal niche. Nature 2009;459:262–265.
25. Miyoshi H, Stappenbeck TS. In vitro expansion and genetic modification of gastrointestinal stem cells in spheroid culture. Nat Protoc 2013;8:2471–2482.
26. Dobin A, Davis CA, Schlesinger F, Drenkow J, Zaleski C, Jha S, Batut P, Chaisson M, Gingeras TR. STAR: ultrafast universal RNA-seq aligner. Bioinformatics 2013; 29:15–21.
27. Anders S, Pyl PT, Huber W. HTSeq–a Python framework to work with high-throughput sequencing data. Bioinformatics 2015;31:166–169.
28. Huang DW, Sherman BT, Tan Q, Collins JR, Alvord WG, Roayaei J, Stephens R, Baseler MW, Lane HC,

Lempicki RA. The DAVID Gene Functional Classification Tool: a novel biological module-centric algorithm to functionally analyze large gene lists. Genome Biol 2007; 8:R183.
29. Huang DW, Sherman BT, Tan Q, Kir J, Liu D, Bryant D, Guo Y, Stephens R, Baseler MW, Lane HC, Lempicki RA. DAVID Bioinformatics Resources: expanded annotation database and novel algorithms to better extract biology from large gene lists. Nucleic Acids Res 2007; 35:W169–W175.
30. Supek F, Bosnjak M, Skunca N, Smuc T. REVIGO summarizes and visualizes long lists of gene ontology terms. PLoS One 2011;6:e21800.
31. Tsui IF, Chari R, Buys TP, Lam WL. Public databases and software for the pathway analysis of cancer genomes. Cancer Inform 2007;3:379–397.
32. Fiorentino M, Ding H, Blanchard TG, Czinn SJ, Sztein MB, Fasano A. Helicobacter pylori-induced disruption of monolayer permeability and proinflammatory cytokine secretion in polarized human gastric epithelial cells. Infect Immun 2013;81:876–883.
33. Schmittgen TD, Livak KJ. Analyzing real-time PCR data by the comparative C(T) method. Nat Protoc 2008; 3:1101–1108.
34. Senger S, Sapone A, Fiorentino MR, Mazzarella G, Lauwers GY, Fasano A. Celiac disease histopathology recapitulates hedgehog downregulation, consistent with wound healing processes activation. PLoS One 2015; 10:e0144634.
35. Jang MH, Kweon MN, Iwatani K, Yamamoto M, Terahara K, Sasakawa C, Suzuki T, Nochi T, Yokota Y, Rennert PD, Hiroi T, Tamagawa H, Iijima H, Kunisawa J, Yuki Y, Kiyono H. Intestinal villous M cells: an antigen entry site in the mucosal epithelium. Proc Natl Acad Sci U S A 2004;101:6110–6115.
36. Albers TM, Moore RP. Use of a lectin as an enterocyte-specific cell surface marker for flow cytometric analysis of isolated native small intestinal epithelial cells. Cytometry 1996;23:72–77.
37. Hacker H, Furmann C, Wagner H, Hacker G. Caspase-9/-3 activation and apoptosis are induced in mouse macrophages upon ingestion and digestion of Escherichia coli bacteria. J Immunol 2002;169:3172–3179.
38. Robinson MD, McCarthy DJ, Smyth GK. edgeR: a Bioconductor package for differential expression analysis of digital gene expression data. Bioinformatics 2010; 26:139–140.
39. Mustata RC, Vasile G, Fernandez-Vallone V, Strollo S, Lefort A, Libert F, Monteyne D, Perez-Morga D, Vassart G, Garcia MI. Identification of Lgr5-independent spheroid-generating progenitors of the mouse fetal intestinal epithelium. Cell Rep 2013;5:421–432.
40. Tsai YH, Hill DR, Kumar N, Huang S, Chin AM, Dye BR, Nagy MS, Verzi MP, Spence JR. LGR4 and LGR5 function redundantly during human endoderm differentiation. Cell Mol Gastroenterol Hepatol 2016;2:648–662 e8.
41. Miyoshi H, VanDussen KL, Malvin NP, Ryu SH, Wang Y, Sonnek NM, Lai CW, Stappenbeck TS. Prostaglandin E2 promotes intestinal repair through an adaptive cellular response of the epithelium. EMBO J 2017;36:5–24.
42. Suh E, Traber PG. An intestine-specific homeobox gene regulates proliferation and differentiation. Mol Cell Biol 1996;16:619–625.
43. Seno H, Miyoshi H, Brown SL, Geske MJ, Colonna M, Stappenbeck TS. Efficient colonic mucosal wound repair requires Trem2 signaling. Proc Natl Acad Sci U S A 2009; 106:256–261.
44. Litvinov SV, Velders MP, Bakker HA, Fleuren GJ, Warnaar SO. Ep-CAM: a human epithelial antigen is a homophilic cell-cell adhesion molecule. J Cell Biol 1994; 125:437–446.
45. Maunoury R, Robine S, Pringault E, Leonard N, Gaillard JA, Louvard D. Developmental regulation of villin gene expression in the epithelial cell lineages of mouse digestive and urogenital tracts. Development 1992; 115:717–728.
46. Finkbeiner SR, Hill DR, Altheim CH, Dedhia PH, Taylor MJ, Tsai YH, Chin AM, Mahe MM, Watson CL, Freeman JJ, Nattiv R, Thomson M, Klein OD, Shroyer NF, Helmrath MA, Teitelbaum DH, Dempsey PJ, Spence JR. Transcriptome-wide analysis reveals hallmarks of human intestine development and maturation in vitro and in vivo. Stem Cell Reports 2015;4:1140–1155.
47. Shouval DS, Ouahed J, Biswas A, Goettel JA, Horwitz BH, Klein C, Muise AM, Snapper SB. Interleukin 10 receptor signaling: master regulator of intestinal mucosal homeostasis in mice and humans. Adv Immunol 2014;122:177–210.
48. Kobayashi K, Hernandez LD, Galan JE, Janeway CA Jr, Medzhitov R, Flavell RA. IRAK-M is a negative regulator of Toll-like receptor signaling. Cell 2002;110:191–202.
49. Carow B, Rottenberg ME. SOCS3, a major regulator of infection and inflammation. Front Immunol 2014;5:58.
50. Dufner A, Pownall S, Mak TW. Caspase recruitment domain protein 6 is a microtubule-interacting protein that positively modulates NF-kappaB activation. Proc Natl Acad Sci U S A 2006;103:988–993.
51. Turksen K, Troy TC. Claudin-6: a novel tight junction molecule is developmentally regulated in mouse embryonic epithelium. Dev Dyn 2001;222:292–300.
52. van der Flier LG, Haegebarth A, Stange DE, van de Wetering M, Clevers H. OLFM4 is a robust marker for stem cells in human intestine and marks a subset of colorectal cancer cells. Gastroenterology 2009; 137:15–17.
53. Liang G, Zhang Y. Genetic and epigenetic variations in iPSCs: potential causes and implications for application. Cell Stem Cell 2013;13:149–159.
54. Levine MM, Bergquist EJ, Nalin DR, Waterman DH, Hornick RB, Young CR, Sotman S. Escherichia coli strains that cause diarrhoea but do not produce heat-labile or heat-stable enterotoxins and are non-invasive. Lancet 1978;1:1119–1122.
55. Ootani A, Li X, Sangiorgi E, Ho QT, Ueno H, Toda S, Sugihara H, Fujimoto K, Weissman IL, Capecchi MR, Kuo CJ. Sustained in vitro intestinal epithelial culture within a Wnt-dependent stem cell niche. Nat Med 2009; 15:701–706.
56. Dotti I, Mora-Buch R, Ferrer-Picon E, Planell N, Jung P, Masamunt MC, Leal RF, Martin de Carpi J, Llach J,

Ordas I, Batlle E, Panes J, Salas A. Alterations in the epithelial stem cell compartment could contribute to permanent changes in the mucosa of patients with ulcerative colitis. Gut 2017;66:2069–2079.
57. van Beelen Granlund A, Ostvik AE, Brenna O, Torp SH, Gustafsson BI, Sandvik AK. REG gene expression in inflamed and healthy colon mucosa explored by in situ hybridisation. Cell Tissue Res 2013;352:639–646.
58. Ouellette AJ. Paneth cell alpha-defensins in enteric innate immunity. Cell Mol Life Sci 2011; 68:2215–2229.
59. Tan X, Hsueh W, Gonzalez-Crussi F. Cellular localization of tumor necrosis factor (TNF)-alpha transcripts in normal bowel and in necrotizing enterocolitis. TNF gene expression by Paneth cells, intestinal eosinophils, and macrophages. Am J Pathol 1993; 142:1858–1865.
60. Sodhi CP, Neal MD, Siggers R, Sho S, Ma C, Branca MF, Prindle T Jr, Russo AM, Afrazi A, Good M, Brower-Sinning R, Firek B, Morowitz MJ, Ozolek JA, Gittes GK, Billiar TR, Hackam DJ. Intestinal epithelial Toll-like receptor 4 regulates goblet cell development and is required for necrotizing enterocolitis in mice. Gastroenterology 2012;143:708–718 e1–e5.
61. Tanner SM, Berryhill TF, Ellenburg JL, Jilling T, Cleveland DS, Lorenz RG, Martin CA. Pathogenesis of necrotizing enterocolitis: modeling the innate immune response. Am J Pathol 2015;185:4–16.

Received August 5, 2017. Accepted January 18, 2018.

Correspondence
Address correspondence to: Alessio Fasano, MD, Mucosal Immunology and Biology Research Center - MGHfC Harvard Medical School 114 16th Street (114-3501), Charlestown, Massachusetts 02129-4404. e-mail: afasano@mgh.harvard.edu; fax: (617) 724-1731.

Acknowledgments
The authors thank S. M. Flaherty for assistance in editing the manuscript, and S. Camhi, clinical research coordinator at Massachusetts General Hospital (Boston, MA), and the medical staff at Massachusetts General Hospital and Brigham and Women's Hospital (Boston, MA), in facilitating the samples collection. The authors are grateful to the Massachusetts General Hospital Next-Generation Sequencing Core in the Department of Molecular Biology for RNA sequencing of samples, and the authors thank Diane Capen for analyzing samples by transmitted electron microscopy at the Massachusetts General Hospital Microscopy Core of the Center for Systems Biology/Program in Membrane Biology.

Accession number of repository for expression data: GSE101531 (https://www.ncbi.nlm.nih.gov/geo/query/acc.cgi?acc=GSE101531). The following secure token has been created to allow review of record GSE101531 while it remains in private status: gncfoiymbjijrml.

Author contributions
Stefania Senger conceived the study, performed the experiments, analyzed the data, and wrote the paper; Laura Ingano, Rachel Freire, and Weishu Zhu performed experiments and analyzed the data; Ruslan Sadreyev conceived the data analysis; Antony Anselmo analyzed the data; Alessio Fasano and William A. Walker conceived the study, analyzed the data, and wrote the paper; and all authors had access to all the data and have reviewed and approved the final manuscript.

Conflicts of interest
The authors disclose no conflicts.

Funding
Supported by National Institutes of Health grants P30 DK-040561, P01-DK033506, U19-AI082655, and R01-DK104344.